Study of amorphous Boron Carbide (a- B_x C) materials using Molecular Dynamics (MD) and Hybrid Reverse Monte Carlo (HRMC)

Khadka Rajan*1, Baishnab Nirmal1, Opletal George2, Sakidja Ridwan1

- 1. Physics, Astronomy and Materials Science Department, Missouri State University, USA
- 2. Data 61 CSIRO, Docklands, Victoria 3008, Australia

ABSTRACT

We present a computational study of amorphous boron carbide (a- B_x C) models using Molecular Dynamics (MD) studied with Stillinger-Weber (SW) and ReaxFF potential. The atomic structure factor (S(Q)), radial distribution function (RDF) and bond lengths comparison with other experimental and ab initio models show that a random arrangement of icosahedra (B_{12} , B_{11} C) interconnected by chains (CCC, CBC) are present in a- B_x C. Subsequently, Hybrid Reverse Monte Carlo (HRMC) method is used to reconstruct a- B_x C structures. The existing SW potential parameters of Boron are optimized for the α -rhombohedral (Icosahedral B_{12}) boron structure using potential energy minimization and incorporated into HRMC. The a- B_x C modeled from MD simulation is used as a sample for experimental input parameters like RDF, S(Q), coordination environments (CO), bond angle distribution (BAD) and bond length (BL) to guide initial configuration and simulation in HRMC. An accurate agreement of structural information between HRMC and MD generated models were found.

Keywords: α-rhombohedral boron, Amorphous Boron carbide, Molecular dynamics, Stillinger-Weber potential, HRMC, Short-Range Order

1. Introduction

Boron carbide is one of the extremely hardest (hardness 30 GPa) materials [1]. It has a high melting point of approximately ~ 2450°C [2] and a low density of 2.52 g/cm³[3]. It is a material of choice for harsh environments because of its extreme hardness, wear-resistant, thermal stability, high melting point and

chemical inertness [4]. It is used as lightweight body armor, as a neutron absorber in the nuclear reactors [5] and as a shielding material [4].

Boron has the unique ability to form caged structures of different sizes [6]. A large variety of boron carbide structure exists depending upon the B/C stoichiometric ratio (from B₄C to B₁₀C) in the structure dictated by carbon concentration [7]. The primitive unit cell of boron carbide consists of a 15-atom system with a 12-atom icosahedral cage having a rhombohedral lattice of trigonal symmetry (R3m space group) and linear chain of 3-atoms connecting icosahedra along the (111) rhombohedral axis [8]. Different variants of boron carbide have been studied and proposed based on symmetry considerations: i) Carbon-rich B₄C (B₁₂C₃)[9], having the structural configuration of B₁₂-(CCC), is the electron-precise form of boron carbide [7] and band calculation suggests this variant be a semiconductor [10]. ii) Boron-rich B_{6.5}C (B₁₃C₂) [9] has the structural configuration of B₁₂-(CBC) with, calculations suggesting a metallic nature [11] which is contrary to experimentally formed boron carbide which is a semiconductor for a wide range of carbon concentration [7]. iii) B₄C having a structural configuration as B₁₁C_p-(CBC) is finally suggested as the most energetically stable variant by theoretical energy minimization [12], [13], where p-stands for the polar site in the icosahedral structure which forms intra-icosahedral bonding with neighboring icosahedra's. It has been theoretically and experimentally agreed upon that B₁₁C_p-(CBC) is the atomic configuration for the stoichiometry of the B₄C and R₃m space group [8].

Small scale ab initio generated structures of amorphous boron carbide suggests the presence of B₁₂, B₁₁C, and B₁₀C₂ icosahedra embedded in the amorphous matrix of boron and carbon [3][14]. Experimentally prepared amorphous boron carbide via chemical vapor deposition (CVD) [3] confirmed the presence of distorted icosahedrons in their sample. Short-range order (SRO) study of a-B₄C thin film deposited by radio frequency (RF) magnetron sputtering assessed using Fourier transform infrared (FTIR) spectra and pair distribution function (PDF) analysis also verified icosahedral presence [15]. Other experimental a-B_xC thin films studied using x-ray absorption near-edge spectroscopy (XANES) [16] and IR & Raman spectroscopy [17] found a random network of icosahedral structure residing inside thin films. Similarly, strain-induced

amorphous boron carbide studied using Raman spectroscopy [18,19] indicated the collapse of the unit cell into icosahedrons and fragments of C and B atoms.

ab-initio MD studies of the SRO of a-B_xC have been done for small scale systems of 120, 135 atoms [14] and 216 atoms [3] but fewer efforts have been made to characterize larger systems due to the limitation of size and computational cost associated with first-principle calculations. Short-range ordering of amorphous boron carbide materials for larger models is needed to fully understand the presence of a network of icosahedrons embedded inside the boron and carbon matrix.

In the present work, the short-range ordering of a-B_xC is studied using Molecular Dynamics. Larger amorphous models of boron carbides of size 10935 atoms as compared to previous ab-initio studies [3,14] are prepared and studied. The amorphous models associated with B₁₂-(CCC), B₁₂-(CBC) and B₁₁C_p-(CBC) are prepared using the Stillinger-Weber (SW) and ReaxFF potentials. The existing SW potential of the B-C system [20] was further modified for icosahedral B-C systems to create these models. Potential energy minimization of α -rhombohedral boron and crystalline B_xC is used to modify the length scaling parameter (σ) and angular cutoffs. Amorphous models generated using the newly parameterized SW and ReaxFF potentials are compared among and with other experimental and first-principle studies. In addition, Hybrid Reverse Monte Carlo (HRMC) equipped with the new SW potential parameters is used to further study the structure of amorphous boron carbide. Real space, reciprocal space and angular information of the new SW generated MD models of amorphous boron carbide is used as structural constraints to guide the HRMC simulation.

2. Theoretical background

2.1. Stillinger-Weber (SW) potential functions

Stillinger and Weber pioneered the empirical form of the interaction potential to describe the condensed phases of silicon which produced the structural and vibrational properties of amorphous silicon [21]. Since then SW potential has been successfully used in modeling single element and multi-element covalent solids

like C [22,23], B [24], B-C [20], B-N [25], Si-N-H [26], In-Ga-N [27], Zn-Cd-Hg-S-Se-Te [28] and many more.

The Stillinger–Weber total energy model is given by the sum of the two-body and three-body interaction terms [21] as

$$E = \sum_{i} \sum_{j>i} V_2(r_{ij}) + \sum_{i} \sum_{j\neq i} \sum_{k>j} V_3(r_{ij}, r_{ik}, \theta_{ijk})$$

The two-body interaction functional form is written as

$$V_{2}(r_{ij}) = \varepsilon_{ij} A_{ij} \left[B_{ij} \left(\frac{\sigma_{ij}}{r_{ij}} \right)^{p_{ij}} - \left(\frac{\sigma_{ij}}{r_{ij}} \right)^{q_{ij}} \right] exp \left(\frac{\sigma_{ij}}{r_{ij} - \sigma_{ij} a_{ij}} \right)$$

Where $a\sigma$ is the cutoff distance for which V_2 vanishes. The three-body interaction potential form as used in LAMMPS [29] is

$$V_{3}(r_{ij},r_{ik},\theta_{ijk}) = \varepsilon_{ijk}\lambda_{ijk}exp\left(\frac{\gamma_{ij}\sigma_{ij}}{r_{ij}-\sigma_{ij}a_{ij}} + \frac{\gamma_{ik}\sigma_{ik}}{r_{ik}-\sigma_{ik}a_{ik}}\right)\left[\cos\theta_{ijk} - \cos\theta_{0ijk}\right]^{2}$$

Here, the subscripts ij represents pair interaction and ijk represents the three-body term. r_{ij} and r_{ik} are the interatomic distances and θ_{ijk} is the angle between bonds ij and ik with i being the central atom. Angle θ_{0ijk} is the angular cutoff for which three-body interaction term vanishes. For the ideal tetrahedral system, θ_{0ijk} is 109.47° . Parameters ε and σ are energy and length scaling parameters to tune cohesive energy and lattice constant of elements under study [30]. Two body and three-body interactions are tuned using A, B, p, q, λ and γ . Two body interaction is invariant upon exchange of indices i and j and three-body interaction term is invariant upon the exchange of second and third indices of ijk [26].

2.2. Hybrid Reverse Monte Carlo (HRMC)

The Hybrid Reverse Monte Carlo (HRMC) method is used to generate the structures of amorphous materials based on the fitting of experimental diffraction information and the minimization of the system

energy using an interatomic potential [31]. It has been used to study the structural properties of amorphous carbon [32–34] and silicon [35] using the interatomic potentials like Environment-Dependent Interatomic potential (EDIP) and SW. HRMC minimizes the error function χ which includes the cost function of each experimental constraint and the energy penalty term for every random displacement of atoms. Before any random atomic movement, the total value of χ [36] is calculated as

$$\chi_{Old,total} = \sum_{i} \left[\frac{\left(S(Q_i)_{exp} - S(Q_i)_{old} \right)^2}{\sigma(Q_i)^2} + \frac{\left(g(r_i)_{exp} - g(r_i)_{old} \right)^2}{\sigma(r_i)^2} \right] + \frac{E_{Old}}{k_B T}$$

Here S(Q) and g(r) are the structure factor and radial distribution function which are obtained from the diffraction experiments. σ represents the uncertainty in ith data point and k_BT is the Boltzmann weighting factor [37]. These weighting factors influence the acceptance probabilities in the HRMC simulation. After the atomic movement, a new total cost function $\chi_{Old,total}$ is calculated and compared with the old one. An atomic movement is accepted if $\chi_{New,total} < \chi_{Old,total}$ and conditionally accepted for $\chi_{New,total} > \chi_{Old,total}$ with the probability $P = exp(\chi_{Old,total} - \chi_{New,total})$ [35,36].

3. SW-potential optimization

3.1. α - rhombohedral boron

Stillinger-Weber (SW) potential parameters for Boron-Boron interactions have been developed by Rasband et.al [38] for B-Si, Dugan et. al [20] for B-C and Moon et. al [25] for B-N. SW potential parameter for boron carbide by Dugan et al. [20] was optimized for stable boron clusters which when applied on icosahedral boron carbide nanoribbon system results in the loss of icosahedral symmetry leading to structural deformation at the temperature of 300 K retaining the structure only at 1 K [39]. Hence, existing B-B interaction σ and $\cos\theta_o$ parameters have been optimized for an icosahedral system using energy minimization. SW potential σ parameter by Dugan et. al was kept constant at 1.418 for all the B-B and C-C interaction affecting the bond lengths of the interacting system. In this study, the σ parameter for the B-B interaction is tuned with energy minimization performed using classical potential utilizing Large-scale

Atomic/Molecular Massively Parallel Simulator (LAMMPS) [29] with an average B-B bond length as the criteria for the choice of parameter. Since icosahedral B₁₂ is the building block of bulk boron and boron carbide structure the average bond length is fitted for α- rhombohedral boron structure. The icosahedral B₁₂ structure has ~39% of the bond angle in between 58°-61° and ~ 38% in between 107°-109° with ~ 20% concentrated at 109°. Thus, the angular cutoff in the SW potential was changed to regular the tetrahedral angle. Then, a supercell of 216 B atoms was constructed from the hexagonal unit cell of α-rhombohedral boron (B₁₂) structure [40]. Conjugate gradient style potential energy minimization was performed on the structure with 0.0 energy tolerance, 1.0e-8 force tolerance, 10⁴ steps of maximum iterations and 10⁶ number of force evaluations. This criterion allows terminating the energy minimization process either with the force tolerance/evaluations or with the maximum no. of iterations defined. This process was applied for all the SW potential σ parameter varied from 1.15 to 1.80. All of the minimization iterations terminated before the maximum no. of 10⁴ steps was reached with force tolerance criterion with an exception of sigma values 1.38 and 1.39. For these two values of sigma we raised the ceiling to 10⁵ steps of maximum iterations and both of them terminated below 10⁵ steps by satisfying the force tolerance criterion like rest of the data points. Then the average bond length B-B of the DFT optimized structure is compared with the SW minimized structure to calculate the difference in the average bond length of the resulting structure. The average B-B bond length (d_{avg}) of the DFT optimized α -boron structure is 1.7705 Å which is same as the literature value reported by Decker et. al [41] and Katada et. al [42] in icosahedra.

Figure 1 shows the plot of the variation of the σ parameter with the modulus of difference in the average bond lengths between the unrelaxed and the SW relaxed structures. Below 1.65, the icosahedral structure

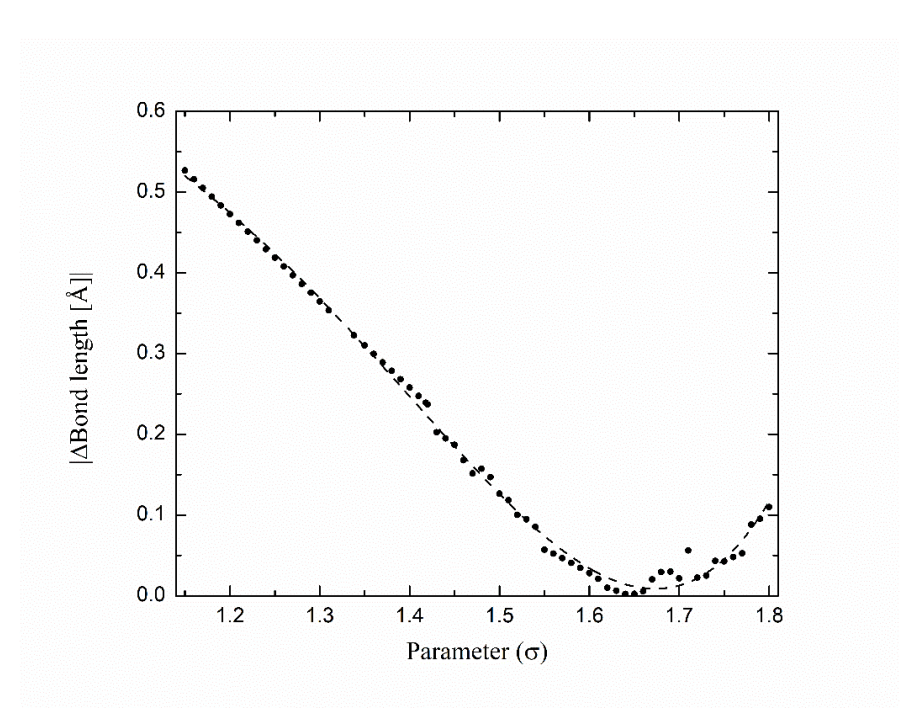


Figure 1 Difference in average bond length of SW minimized α -boron structure with the variation of SW potential σ parameter.

Table 1 Average bond lengths of boron clusters calculated using Old SW, New SW and Ab initio generated structures.

Boron Clusters	Average bond leng	gth (Å)	∆Bond Length (Å)		
n	Ab initio $(d_{o,avg})$	$\operatorname{Old}\operatorname{SW}\left(d_{old,avg}\right)$	New SW $(d_{new,avg})$	$\mid d_{o,avg}$ - $d_{old,avg}\mid$	do,avg - dnew,avg
B ₇	1.6937	1.43882	1.64993	0.25488	0.04377
B ₁₀	1.68781	1.42711	1.6423	0.2607	0.04551
B ₁₂	1.68244	1.42987	1.64885	0.25257	0.03359
B ₁₄	1.68492	1.43167	1.65001	0.25325	0.03491
B ₁₆	1.68621	1.44034	1.65651	0.24587	0.0297
B_{18}	1.68504	1.43764	1.65573	0.2474	0.02931
B_{20}	1.6671	1.42412	1.63849	0.24298	0.02861
B_{26}	1.69544	1.47123	1.69597	0.22421	0.00053
B ₄₄	1.68158	1.44938	1.66898	0.2322	0.0126
B_{80}	1.71349	1.46555	1.69089	0.24794	0.0226

contracts resulting in the increased error in bond length. And above 1.65, the icosahedral structure expands moving away from the d_{avg} value of α -boron. At the original SW σ value of 1.418, d_{avg} was found to be 1.53144 Å with the difference of 0.23901 Å whereas, with the new optimized σ value of 1.65, d_{avg} was calculated to be 1.77259 Å with the difference of only 0.0021 Å. Hereafter the SW parameter by Dugan et. all will be called the Old SW and the modified form with σ =1.65 and θ_o = 109.47° will be called henceforth the New SW.

For both the Old and the New SW, the B-B interaction parameters were used to predict the average bond length of the boron clusters ranging from B_7 to B_{80} . The structural relaxation of stable boron clusters B_7 , B_{10} , B_{14} , B_{16} , B_{18} [43], B_{12} , B_{20} , B_{26} , B_{80} [44], B_{44} [45] was performed as described earlier and the average bond lengths computed and compared against the DFT calculated values as listed in Table 1. During minimization, the structural geometry is conserved with only a change in bond lengths between the boron atoms. As seen from Table 1 bond length error due to Old SW in all the cases of boron clusters are found to be greater than 0.22 Å and bond length error in case of the New SW are lower than 0.05 Å. Overall, the d_{avg} results obtained with the New SW B-B interaction parameters are in good agreement with the Ab initio values for boron clusters.

3.2. Boron carbide crystal

Boron carbide crystal is a complex crystal structure where different bond angles are present for different variants as shown in Figure 2. The three-body angular cut off $(cos\theta_{oijk})$ in the SW potential will be different for the different crystal structures of boron carbide. For the two-element system, there are three two-body pairs namely B-B, C-C, and B-C. There are eight combinations of three-body parameters namely B-B, C-C-C, B-C-C, C-B-B, B-B-C, C-B-C, C-C-B and B-C-B where the first atom is the central atom with others on two sides. Here, all the three body angular cutoffs $(cos\theta_{oijk})$ are obtained from the crystal structure of boron carbide and cutoffs for linear chains- such as CCC and CBC chain is used a value of 180° in all the

Table 2 SW potential parameters for B12-(CCC) used in LAMMPS.

Pairs	3	σ	а	λ	γ	$cos(\theta_o)$	A	В	p	q	tol
B-B-B	1.00	1.650	1.8179	1.00065	0.32408	-0.3333	13.4487	0.08477	4.0	0.0	0.0
C-C-C	1.00	1.418	1.8945	18.70790	1.20000	-1.0000	5.37900	0.50820	4.0	0.0	0.0
В-С-С	1.00	1.650	1.8562	4.32667	0.62362	-1.0000	8.50533	0.20756	4.0	0.0	0.0
С-В-В	1.00	1.650	1.8562	4.32667	0.62362	-0.4226	8.50533	0.20756	4.0	0.0	0.0
В-В-С	1.00	0.000	0.0000	2.08074	0.00000	-0.4695	0.00000	0.00000	0.0	0.0	0.0
С-В-С	1.00	0.000	0.0000	8.99683	0.00000	-0.2250	0.00000	0.00000	0.0	0.0	0.0
С-С-В	1.00	0.000	0.0000	8.99683	0.00000	-0.2250	0.00000	0.00000	0.0	0.0	0.0
В-С-В	1.00	0.000	0.0000	2.08074	0.00000	-0.4695	0.00000	0.00000	0.0	0.0	0.0

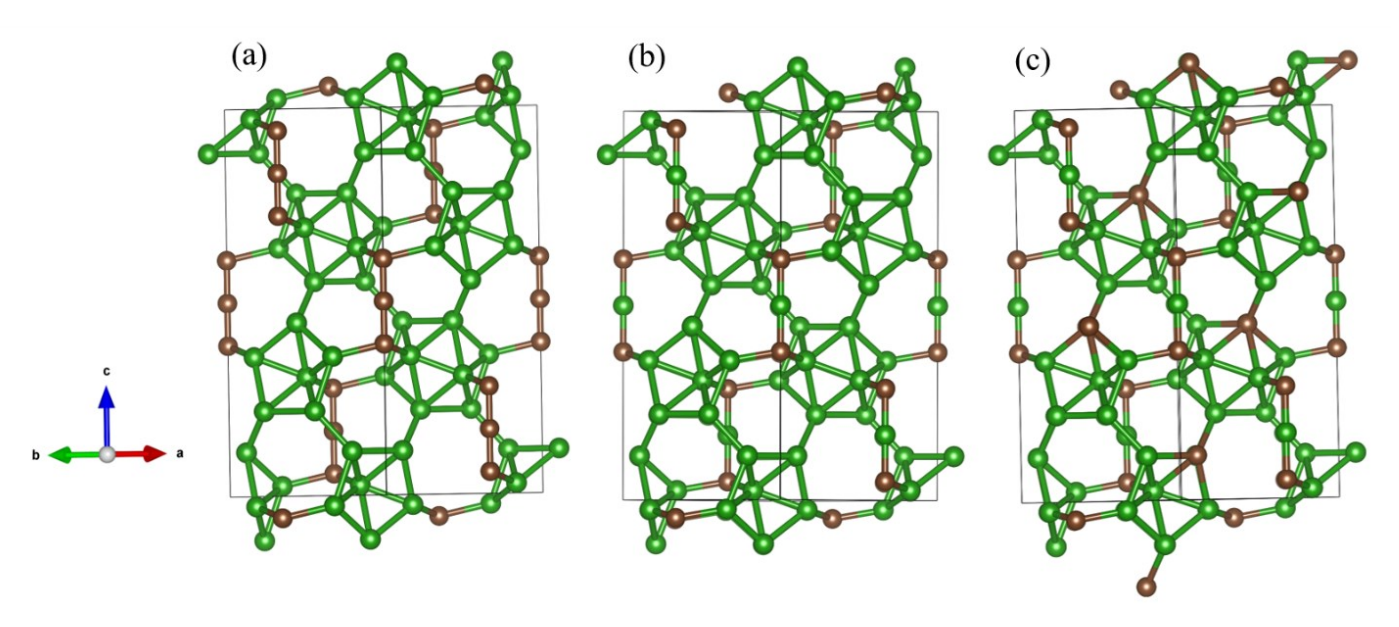
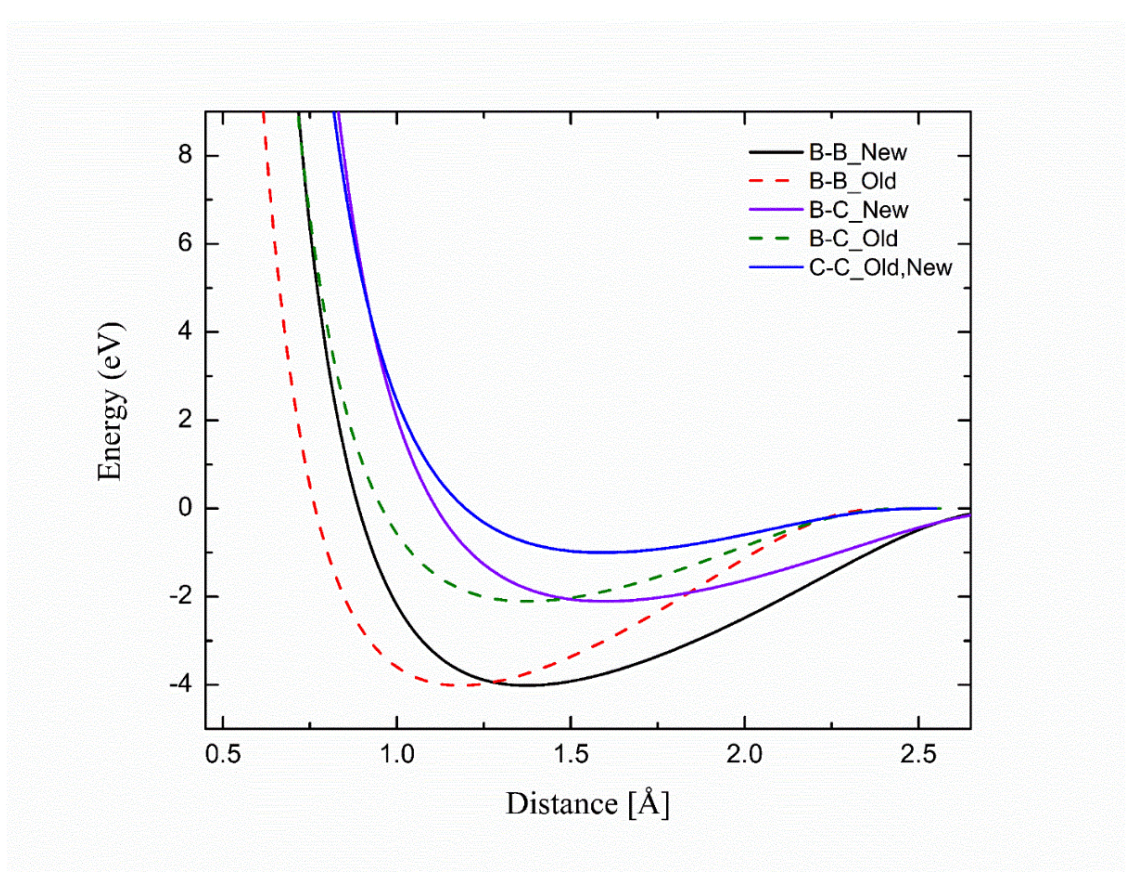


Figure 2 Boron carbide crystal structure with hexagonal unit cells. B atoms are green and C atoms are brown. (a) B_{12} -(CCC). (b) B_{12} -(CBC). (c) $B_{11}C_p$ -(CBC).

variants of boron carbide. If the particular angular type is missing in the crystal structure eg. C-B-C in B₁₂-(CBC) then regular tetrahedral angular cutoff is used. σ is kept constant at 1.65 for three-body pairs B-C-C and C-B-B whose second and third elements are the same. All other parameters for B-C-C and C-B-B are the same as that of Dugan et. al [20]. The parameters ε and λ for the three-body interactions with different second and/or third elements e.g. for B-C-B are calculated using the geometric parameter mixing rule i.e., $\varepsilon_{B-c-B} = \sqrt{\varepsilon_{B-B}\varepsilon_{B-C}}$ and $\lambda_{B-c-B} = \sqrt{\lambda_{B-B}\lambda_{B-C}}$. This rule has been widely used to calculate cross parameter terms in LJ potential as Berthelot rule [46]. The other parameters, namely, A, B, p, q, σ , a, γ of B-C-B type three-body interaction are assumed to be negligible and set to zero following the LAMMPS documentation [47]. The complete set of parameters we obtained using the above-discussed methodology for B₁₂-(CCC) are listed in Table 2. The *tol* parameter in the last column is defined in LAMMPS for further optimization for the cutoffs [47]. The SW potential parameters for B₁₂-(CBC) and B₁₁C_p-(CBC) are provided in the supplemental material.

The potential energy plots of the two body SW potential energy comparisons between the Old SW and the New SW for all the interactions present in the boron carbide system namely B-B, B-C and C-C are shown in Figure 3. The potential well minimum shifts towards a longer separation for the New SW in case of both the B-B and B-C interactions whereas the C-C curve remains unaffected. The shift in B-B is ~ 0.21 Å and B-C is ~ 0.12 Å which is due to the change in the length scaling parameter σ parameter from 1.418 to 1.65 which ultimately changes the two-body cutoff $a\sigma$. The shift in the potential is responsible for predicting the correct bond lengths for the boron carbide system with the New SW parameters compared to Old SW. The DFT optimized structures of B₁₂ [40], B₁₂-(CCC) [48], B₁₂-(CBC) [49] and B₁₁C_p-(CBC) [3] were potential energy minimized as described above using the New SW, Old SW and ReaxFF potential [50]. Table 3 shows the d_{avg} predicted by DFT, ReaxFF, New SW and Old SW potential for all the bonds present in the structures.



 $Figure\ 3\ Stillinger-Weber\ potential\ two-body\ energy\ for\ B-B,\ B-C\ and\ C-C\ bonds\ comparison\ between\ Old\ SW\ and\ New\ SW\ parameters.$

Table 3 Average bond length comparison of B_{12} , B_{12} -(CCC), B_{12} -(CBC), B_{12} -(CBC) and $B_{11}C_p$ -(CBC) predicted using DFT, ReaxFF, New and Old SW potential.

	B-B			B-C				C-C				
Stoichiometry	DFT	ReaxFF	New SW	Old SW	DFT	ReaxFF	New SW	Old SW	DFT	ReaxFF	New SW	Old SW
B ₁₂	1.770	1.807	1.798	1.531	-	-	-	-	-	-	-	-
B ₁₂ -(CCC)	1.773	1.756	1.731	1.559	1.664	1.711	1.721	1.708	1.333	1.292	1.693	1.700
B ₁₂ -(CBC)	1.799	1.771	1.780	1.557	1.562	1.611	1.664	1.674	-	-	-	-
$B_{11}C_p$ -(CBC)	1.732	1.761	1.762	1.551	1.659	1.644	1.633	1.551	1	ı	1	1.633

From Table 3 it can be seen that the B-B bond length of the DFT optimized structure is very close to that of ReaxFF and New SW minimized structures with an error of ~±0.02 Å. Whereas, Old SW predicted a B-B bond length for the structure ~0.22 Å smaller than the DFT relaxed structure. This is due to the contraction of the icosahedral structure due to the Old SW B-B potential parameters. The B-C bond length is overapproximated by all the potentials in the case of B₁₂-(CCC) and B₁₂-(CBC) in comparison to DFT optimized geometry. In the case of the B₁₁C_p-(CBC) crystal structure, the B-C bond length prediction by ReaxFF and New SW potential are 1.644 Å and 1.633 Å respectively which is very close to that of DFT value 1.659 Å. In comparison, the Old SW generated relaxed structure yields the B-C length of 1.551 Å which is much shorter in comparison to that from the New SW potential. Although B₁₁C_p-(CBC) is the stable variant of boron carbide crystal, the Old SW – based minimized structure was not able to stabilize such a geometry. This further confirms our approach to model these which is quite comparable to that achieved by the ReaxFF-based minimization. In the case of Old SW during the minimization process, some of the C atoms which were initially resided in the icosahedra would leave its icosahedral site and form bonds with the CBC chain atom resulting in an increase in the C-B bond count and new C-C bond which was initially absent (see Figure 4a). In contrast, the C-atom remains bonded within the icosahedra during the New SW minimization (see Figure 4b). We should note however that the C-C bond length prediction for B₁₂-(CCC) for both the New SW and the Old SW has the same level of error as when the interaction parameters were kept unchanged except for the angular cutoff correction. Nevertheless, overall, the New SW potential of boron carbide obtained by modifying the parameters based on the icosahedral-based geometry of the crystal was able to produce results close to that of the sophisticated ReaxFF potential.

The bond angle distribution $B(\theta)$ is the first nearest neighbor angle histogram that can be used to measure the quality of the structure. Figure 5 shows the $B(\theta)$ of boron carbide crystal optimized using DFT and

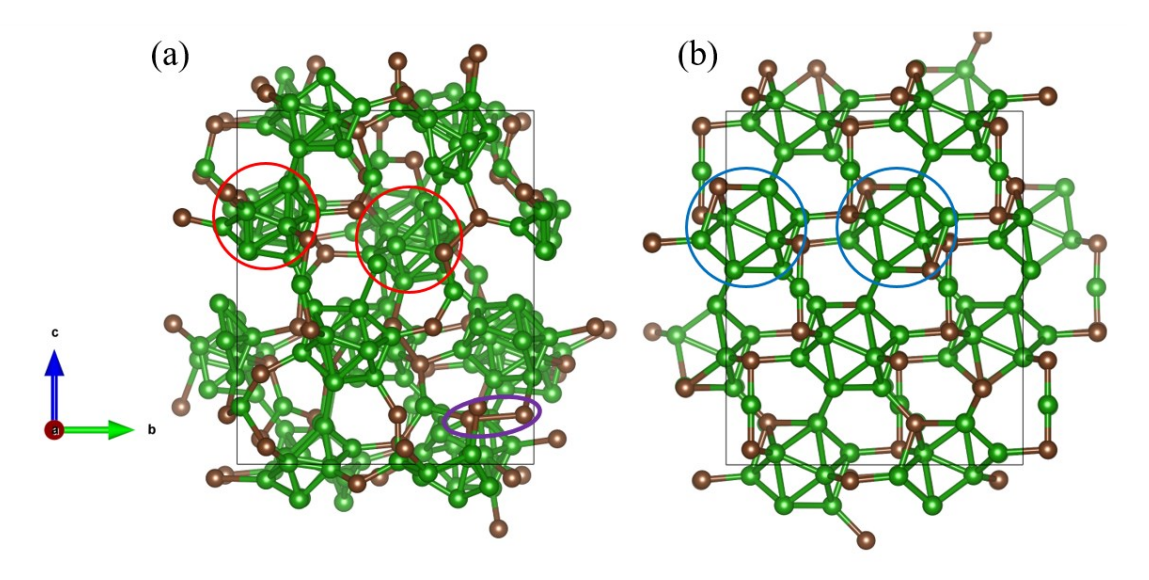


Figure 4 Old SW and New SW potential optimized structure of $B_{11}C_p$ -(CBC). The icosahedral structure opened up during the minimization process for Old SW. Open icosahedral cages are circled red and the C-C bond circled purple. Green sticks are the B-B bonding and Brown sticks are C-C bonds. (a) Old SW minimization (b) New SW minimization.

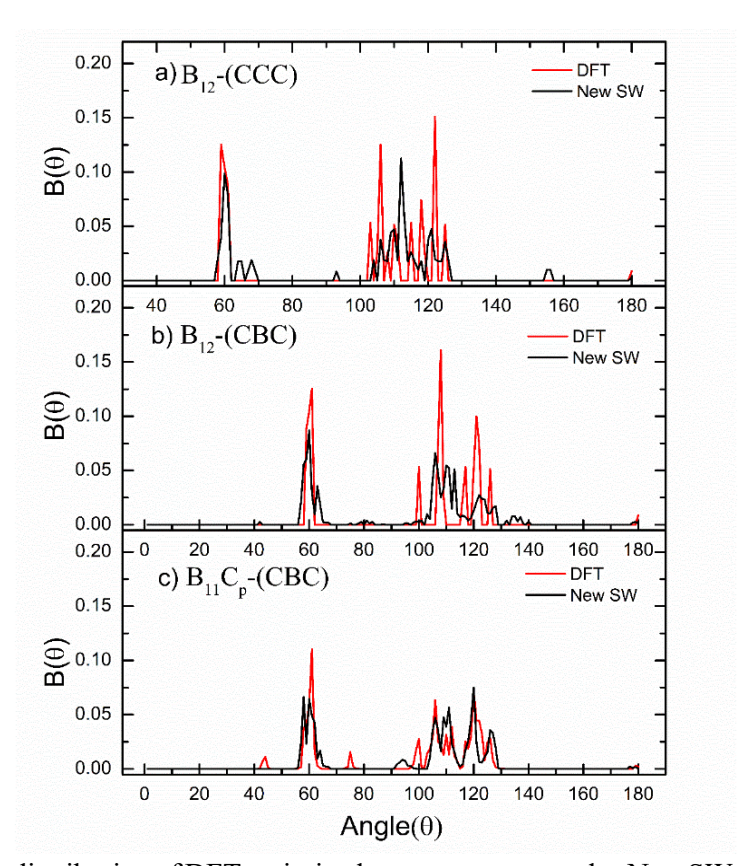


Figure 5 Bond angle distribution of DFT optimized structure compared to New SW minimized boron carbide crystal structure.

New SW potential. In all the cases, the angular distribution is centered around two peaks, one at an angle 60° and the other between 100° - 130° . B(θ) around 60° is in good agreement in all the cases and comes from the three-membered B-atoms rings in the triangles forming icosahedrons. Small peaks at 180° in all the cases come from the atomic chains (CCC and CBC) present in the crystal structure. SW potential function is limited to only one angular cutoff ($\cos\theta_{oijk}$) per three-body interaction type. It is due to this inherent limitation of SW potential function all the angular peaks present in DFT optimized structure aren't present in the SW minimized structure.

4. Computational details

4.1. Amorphous boron carbide – MD

Amorphous models of B₁₂-(CCC), B₁₂-(CBC) and B₁₁C_p-(CBC) were studied using the New SW and ReaxFF potentials in the LAMMPS simulation package. To study the short-range order of icosahedrons in the matrix of boron and carbon atoms as seen in the smaller theoretical models and experimentally studied samples we packed icosahedrons and chain atoms in a box with the random arrangement. In order to make the three a-B_xC samples, 729 units of icosahedrons and chain atoms containing 10935 atoms were packed randomly inside the simulation cell of dimension $\sim (45.80 \times 45.80 \times 45.80)$ Å³ with the minimum distance between the atoms to be 1.9 Å using PACKMOL [51]. The initial density of all the packed disordered structures was ~ 0.114 atoms/Å³ (~ 2.09 g/cm³). Classical MD simulation was performed on these samples with periodic boundary conditions applied in all three directions. The three initial randomly packed models of boron carbide were subjected to constant pressure and temperature (NPT) simulation using the ReaxFF potential for 42.5 ps from 10 K to 300 K with 0 Gpa and equilibrated at 300 K for 82.5 ps with the time step of 0.25 fs. With the New SW potential, we applied a pressure scheme where constant volume and temperature (NVT) and NPT simulations with different pressures applied with the goal of matching the density. This scheme was applied to densify the structure using New SW to get reasonably close to the density of the ReaxFF model produced earlier and to compare the short-range order characteristics among the models. Here, firstly NVT simulation was performed for 50 ps at 300K followed by NPT simulation at

300 K with varying pressure from 0 Gpa to 20 Gpa for 550 ps. We have added this scheme as part of our supplemental materials. It is important to note that the final structure is free from residual stress since it was released with the NPT simulation at zero pressure. A similar approach has been found in the literature and applied to get the desired density of the material for comparison to experiment [52]. The six different a-B_xC models were prepared using two different interatomic potentials and compared. These models are compared in terms of their final density (ρ), bond angle distribution (B(θ)), radial distribution function (g(r)), structure factor (S(Q)) and the bonding environment.

4.2. Amorphous boron carbide – HRMC

HRMC simulation is employed to reconstruct the amorphous models of boron carbide prepared using the MD simulation detailed above. The radial distribution function and static structure factor are calculated from the previous MD models of a-B_xC and used in place of experimental constraints within HRMC. The 3D reconstruction of the amorphous models of materials based only on 1D diffraction data is challenging for HRMC simulations [53]. Even if we apply multiple constraints along with diffraction data fitting in the simulation process to find the 3D atomic structure starting from the completely random configuration of atoms, the solution will be different after every simulation because of a huge family of solution. So, to fit the structure with the diffraction data, the initial starting model cannot be a random collection of atoms. As suggested in the previously discussed literature of amorphous boron carbides where icosahedrons are in the matrix of boron and carbon atoms, we packed another set of icosahedrons and chain atoms randomly in the simulation cell as initial starting configuration for HRMC simulation.

In this HRMC study, we have packed 729 icosahedrons and chain atoms with the minimum tolerance distance of 1.9 Å in a simulation cell of dimension (43.37X43.45X43.40) Å³ to contain 10935 atoms. This structure was energetically minimized at 300K for 2 x 10⁶ steps using New SW equipped potential in the HRMC code to find the local minimum of the Potential Energy Surface (PES). The output is then fitted with the calculated diffraction data together with the potential constraint. The two-stage HRMC modeling approach has been previously applied in predicting the structure of amorphous materials [53,54]. The output

structure of stage-1 is fitted with S(Q), g(r) and $B(\theta)$ along with the average bond length, and coordination histogram constraint since at least four constraints are recommended for multi-element

Table 4 Percentage of the angular type present in the amorphous models of boron carbide samples prepared using New SW and ReaxFF potential.

Bond	a-B12-(CC	C)	a-B12-(CB	C)	a-B11Cp-(CBC)		
Angles	New SW	ReaxFF	New SW	ReaxFF	New SW	ReaxFF	
B-B-B	94.14	84.48	96.27	82.29	93.70	64.26	
В-В-С	4.78	9.49	3.09	11.33	5.14	22.03	
B-C-C	0.00	0.01	0.00	0.74	0.01	1.59	
С-В-В	0.10	1.43	0.09	4.41	0.19	9.98	
С-В-С	0.42	2.78	0.26	1.01	0.50	2.00	
C-C-C	0.24	1.44	0.00	0.00	0.14	0.00	

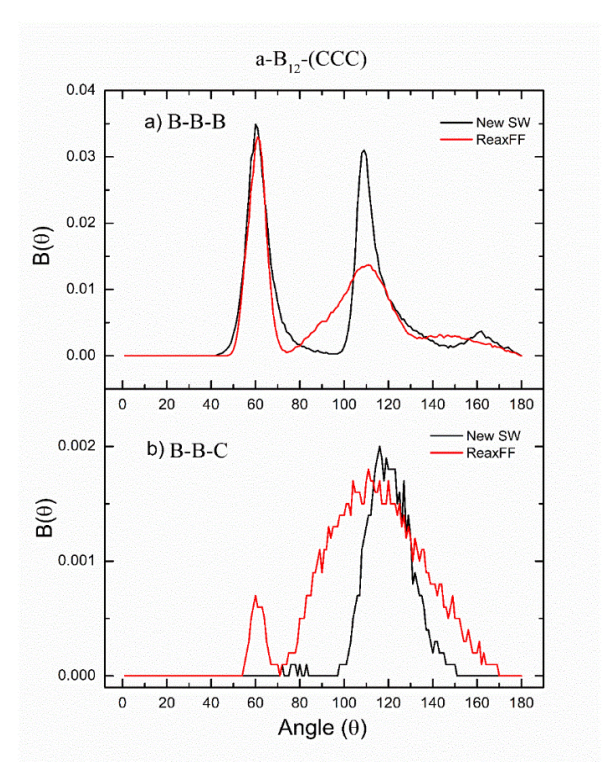


Figure 6 B-B-B and B-B-C type bond angle distribution comparison of a-B12-(CCC) structure between New SW potential and ReaxFF.

HRMC simulation [55]. A quenching approach is used during the fitting process which starts from 1000K and is linearly quenched down to 800K, 500K, and 300K in four subsequent stages where every stage takes 25% of the total simulation steps. All the HRMC simulations are carried out for 10⁷ steps to generate the fitted amorphous models.

5. Results

5.1. Structure of amorphous boron carbide- MD

5.1.1. Bond Angle Distribution ($B(\theta)$)

For the two-element system, there are six different possible combinations of bond angles that can be present in the structure. Table 4 lists all the types of bond angles with their respective amounts present in all the three different variants of amorphous boron carbide models. It can be seen that the prominent angular type present in the amorphous models of boron carbide samples are B-B-B, B-B-C, C-B-B, and C-B-C. The bond angles B-C-C and C-C-C are less than 2% in all the amorphous samples. Figure 6 shows the comparison between New SW and ReaxFF for the two prominent angular type B-B-B and B-B-C in a-B₁₂-(CCC) sample. It can be seen that at around 60° the distribution for B-B-B type is equivalent for both the potential whereas in the higher angular region ReaxFF allows wide distribution of angle around $\sim 110^{\circ}$ compared to SW.

The bond angle distributions of B-B-B and B-B-C types are presented in Figure 7 for two other models of boron carbide. Here, a similar observation can be made in terms of the B-B-B angle as in a-B₁₂-(CCC). However, B-B-C is more prominent in the ReaxFF generated models than before with the B-B-C angle distribution having a sharp peak at around 60° in the case of a-B₁₁C_p-(CBC) structure compared to other amorphous models. The origin of this peak comes from the fact that one of the C atoms in the structure is a part of icosahedra forming near equilateral angles with B atoms. The absence of this prominent peak in the New SW created model indicates that some of the C atoms in the icosahedra are leaving the site and forming the bonding with the other atoms. In fact, it is seen in Table 4 as a C-C-C angle which is absent in

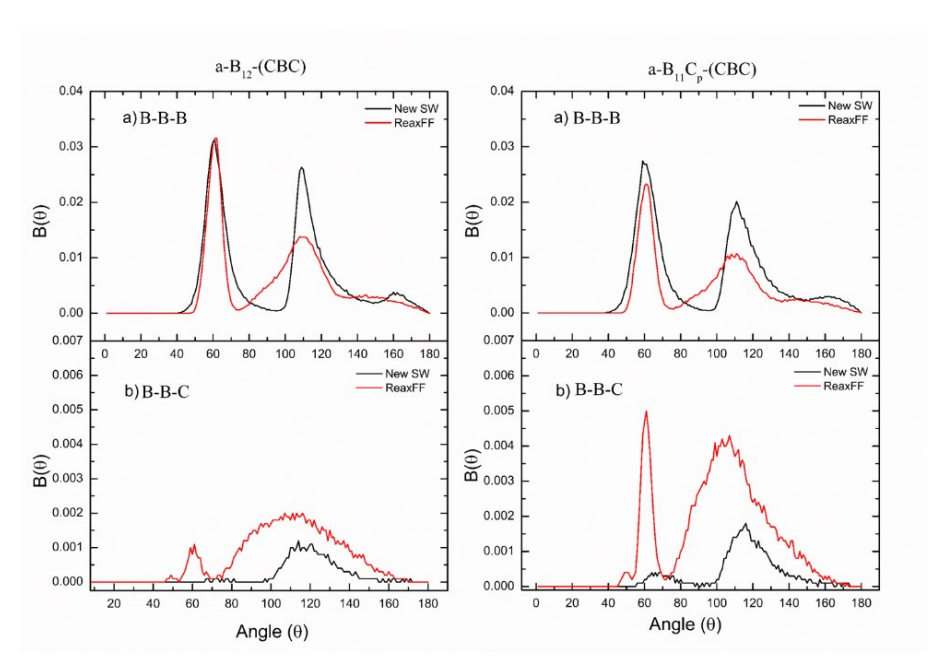


Figure 7 B-B-B and B-B-C angular type comparison between New SW and ReaxFF generated a- B_{12} -(CBC) and a- $B_{11}C_p$ -(CBC), amorphous models.

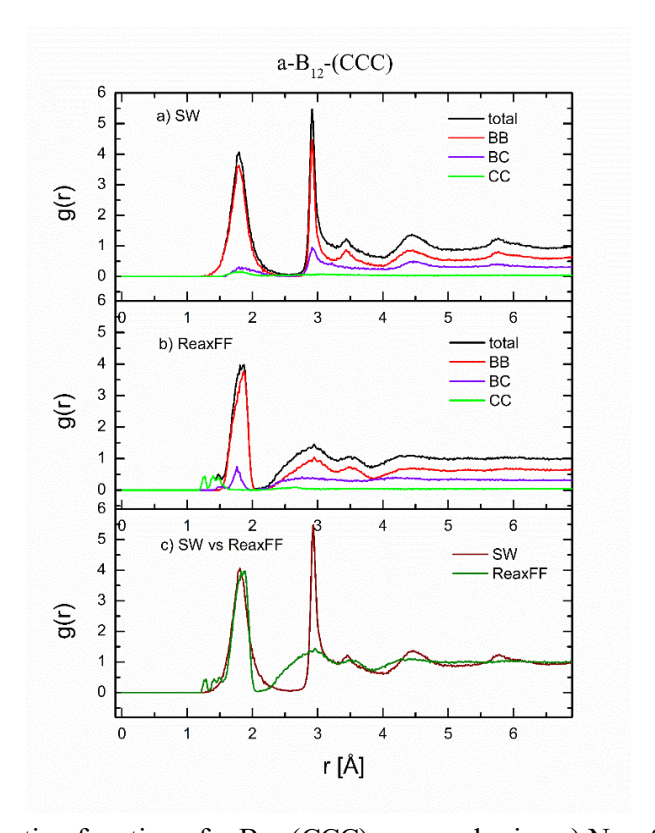


Figure 8 Radial distribution function of a- B_{12} -(CCC) prepared using a) New SW b) ReaxFF and c) comparison between New SW and ReaxFF generated total RDF.

the ReaxFF generated model. This strong peak could potentially be used as a signature to identify whether or not C-atom is within the icosahedral sites in the unknown amorphous boron carbide sample.

5.1.2. Radial distribution function (g(r)) and Structure factor (S(Q))

Radial distribution function g(r) provides information on the short-range order of the material structure under study. Figure 8 shows g(r) of a-B12-(CCC) using New SW and ReaxFF potential. The sharp first peaks at ~1.8 Å on both the models as seen in Figure 8 (a) and (b) is due to B-B pair with only minor difference noted in Figure 8 (c). This suggests the strong short-range order presence in the structure is predominantly due to B-B pairs. The second nearest neighbor peak, largely due to B-B pairs, is found at ~2.9Å for both potentials. The New SW potential generates a sharp distribution while ReaxFF results in broader distribution. This tells us that the second nearest neighbors have a wide distribution of bond lengths in the ReaxFF model whereas the New SW model has a much more similar bond length giving rise to the sharp peak. Although it looks erroneous at first sight, this signal can be easily explained using the nearest neighbor distances shown in Figure 9.

The first B-B peak icosahedra arise from B_R - B_R type pairs while the second neighbor peak caused by the B_G - B_G pair and the third peak by B_Y - B_Y pairs. The B_G - B_G pair distance is around ~2.9 Å within the icosahedra and is responsible for the second peak in the g(r) which is present in both models. The root cause for the strong peak for the New SW potential in the g(r) seen in Figure 8 (a) and 10 (a) lies in the functional form of SW potential where only one angular cutoff can be applied for one element type. Figure 6 and Figure 7 show the towering peak of the New SW model compared to ReaxFF model at ~110° which comes from the bond angle B_R - B_G - B_G type in Figure 9 resulting in the length of B_G - B_G type to peak at ~2.9 Å. As ReaxFF allows a wide variety of B_R - B_G - B_G type angles there is a broad peak for B_G - B_G type neighbors in g(r). The second neighbor peak in New SW generated model is, in fact, an indication of the presence of pentagonal rings coming from icosahedra in the amorphous boron carbide model. Additionally, the B_Y - B_Y lengths are responsible for the tiny shoulder peak at ~3.4Å which is seen in both Figure 8 (a) and (b). As shown in Figure 8 (a) B-C pairs have first, second and third peaks around B-D position whereas B-C peak

in Figure 8 (b) is more prominent and presents only around \sim 1.75Å. The prominence of this peak on ReaxFF made a-B₁₂-(CCC) for the B-C pairs is due to the CCC chain atom connecting the icosahedrons which are in agreement with the higher density of ReaxFF model compared to that of New SW model discussed later. The amount of carbon atoms in the amorphous model is 20% which is reflected as a very low-intensity peak at \sim 1.80Å in Figure 8 (a) and around \sim 1.4Å in (b). This mismatch in C-C position arises because New SW has already been shown to overestimate C-C bond length in Table 3. C-C pairs form the shoulder peak to the left of the first peak of global g(r) in case of ReaxFF model.

Figure 10 shows the RDF of two other amorphous model a-B₁₂-(CBC) and a-B₁₁Cp-(CBC). All the B-B peaks are located almost around the same position indicating the short-range ordering of icosahedral structure in the amorphous matrix environment. The presence of the B-C pair is more prominent in a-B₁₂-(CBC) and even stronger in $a-B_{11}C_p$ -(CBC) model in case of both the potentials. This presence is expected as every chain atom present in the structure has B-C pairs compared to the CCC chain in a-B₁₂-(CCC) where the B-C interaction arises only between icosahedra and chain atoms. However, the B-C peaks are present at ~ 1.45 Å and ~ 1.75 Å compared to only at ~ 1.75 Å in ReaxFF a-B₁₂-(CCC) model. These two peaks arise from different types of B-C bonding environment. The smaller length arises from the B-C bonds in the chain atoms whereas longer bond arises from C in the CBC chain and B in the icosahedra [56] in Figure 10 (b) a-B₁₂-(CBC). But in the case of Figure 10 (b) a-B₁₁C_p-(CBC) there is C atom within in icosahedra which adds more types of B-C bonding environment in addition to the present in Figure 10 (b) a-B₁₂-(CBC). The further additions are inter-icosahedral B-C pairs and intra-icosahedral B-C pairs [17] both of which add ~1.75Å type bond length giving rise to the sharp peak even in the global g(r). As seen in Figure 10 (b) both on the left and right C-C pairs peaks at around ~1.2 Å due to the bonding between C-atoms from two CBC chains present in the amorphous structure. But C-C pair is in higher amount in Figure 10 (b) a-B₁₁C_p-(CBC) compared to Figure 10 (b) a-B₁₂-(CBC) as there is additional bonding between C-atom in B₁₁C_p and CBC chain carbon and intra-icosahedral bonding that connects two B₁₁C_p. The simplicity of SW potential formulation couldn't differentiate between the B-C pairs in CBC and B-C pairs between chain carbon and

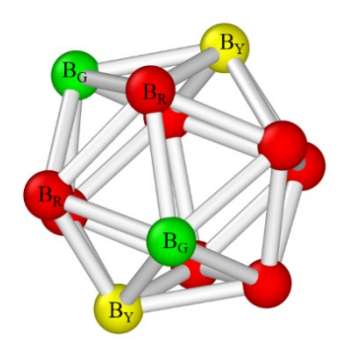


Figure 9 Nearest neighbor distances present in the B_{12} icosahedra. Here red, green and yellow colored boron atoms are used to show the first, second and third nearest neighbor distances respectively present in B_{12} icosahedra. Here, B_R - B_R = 1st neighbor, B_G - B_G = 2st neighbor and B_Y - B_Y = 3rd neighbor.

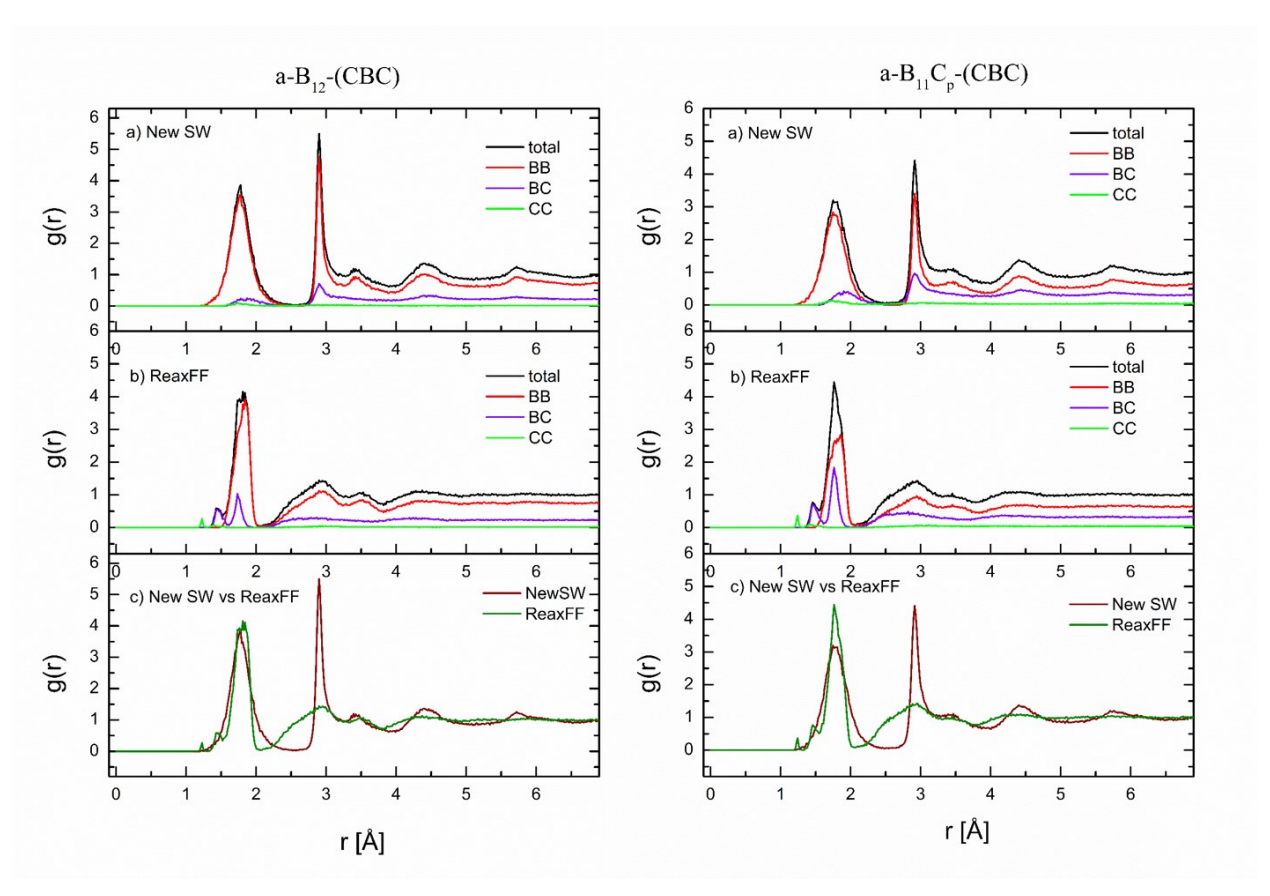


Figure 10 Radial distribution function of a- B_{12} -(CBC) (left) and a- $B_{11}C_p$ -(CBC) (right) prepared using a) New SW b) ReaxFF and c) comparison between New SW and ReaxFF generated total RDF.

icosahedral boron with a broad and diffused peak at ~1.85Å in Figure 10 (a). Presence of C-C pairs is very minimal in New SW generated model in Figure 10 (a).

Neutron diffraction static structure factor (S(Q)) is a reciprocal space property of materials that are often used to characterize disordered glasses [57–60]. S(O) in reciprocal space is a Fourier transform of g(r) in real space which carries short-range, medium-range and nano-order structural information [60]. In Figure 11 we report the total structure factor of a- B_{12} -(CCC) samples and its comparison with the S(Q) of Randomly packed B_{12} and DFT structure in the literature within $0.45 \le Q \le 21 \text{ Å}^{-1}$. Icosahedral B_{12} was packed in a simulation box and the structure factor was computed and carries signature peaks containing information of the disordered boron icosahedra. S(Q) values below 1Å⁻¹ are not experimentally reliable due to detector resolution and contain unphysical oscillation [37], and are thus excluded from the interpretation. Figure 11 shows the first small intensity peak at $\sim 1.5 \text{ Å}^{-1}$ in all cases with more intensity for Random B₁₂. The shoulder peak located at $\sim 2.6 \text{ Å}^{-1}$ is prominent only in New SW and the DFT generated a-B_{2.5}C (B₁₅₄C₆₂) model [3]. The second peak has the highest intensity compared to any other peak in S(Q) located at ~4.6 Å-1 for New SW and ReaxFF models with New SW having a very strong signal. Random B₁₂ has a peak shifted to the left at $\sim 4.4 \,\text{Å}^{-1}$ compared to DFT a-B_{2.5}C which has right-shifted peaks at $\sim 4.9 \,\text{Å}^{-1}$. As this second peak is a high-intensity peak present in all the models having random icosahedrons in the amorphous matrix and experimental thin film of boron carbide [3], this can be used as a signature of disordered icosahedrons. The third peak for Random B_{12} is present at $\sim 7.2 \text{ Å}^{-1}$ with a small shoulder at ~ 9 Å-1 but New SW model has two split peaks at both positions while ReaxFF has a peak in between at \sim 7.7 Å⁻¹. DFT model a-B_{2.5}C has just a plateau from \sim 6.5 to 10 Å⁻¹ but interestingly experimental boron carbide thin film by Pallier et. al. [3] has two split peaks in the same position as seen in New SW. Afterward, DFT a-B_{2.5}C peak dampens rapidly followed by ReaxFF model. Random B₁₂ peaks have oscillating peaks that dampen much later than New SW peaks. These oscillating dampening peaks in S(Q) are often seen on disordered amorphous glasses [60,61]. Figure 12 includes all the amorphous boron carbon models prepared

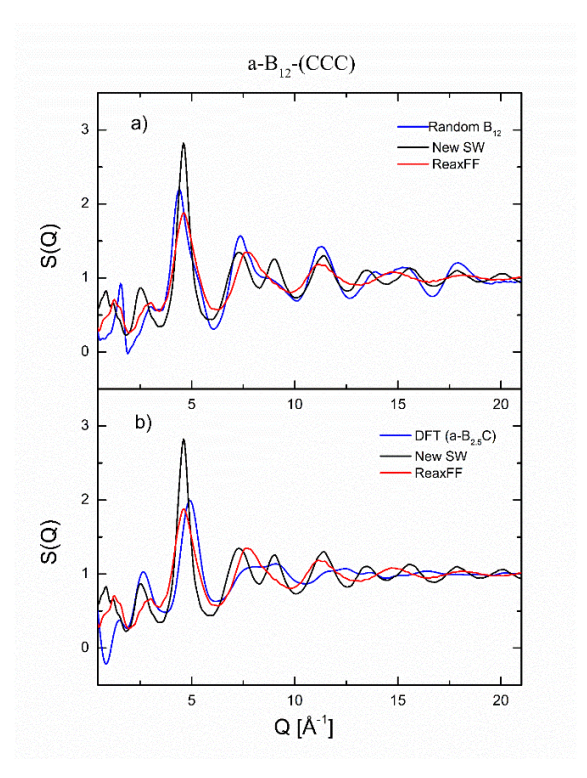


Figure 11 Total structure factor of amorphous boron carbide a- B_{12} -(CCC) prepared using New SW (black line) and ReaxFF (red line) and their comparison with the (a) S(Q) of Random B_{12} (blue line) (b) DFT a- $B_{2.5}$ C [3] (blue line).

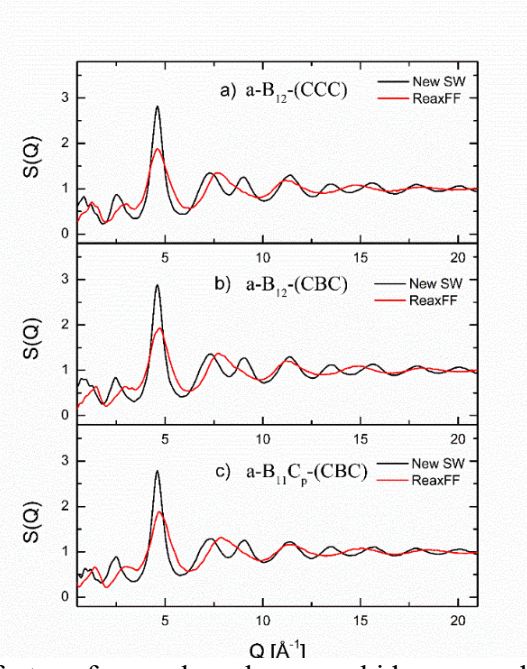


Figure 12 Total structure factor of amorphous boron carbide prepared using New SW (black line) and ReaxFF (red line) (a) $a-B_{12}$ -(CCC) (b) $a-B_{12}$ -(CBC) (c) $a-B_{11}C_p$ -(CBC).

using New SW and ReaxFF. The features of S(Q) of both New SW and ReaxFF model in Figure 12 (b) and (c) are similar and consistent with the explanation of a- B_{12} -(CCC). The S(Q) in Figure 12 (b) and (c) suggests the amorphous environment in terms of short-range order are similar to a- B_{12} -(CCC).

5.1.3. Structural units

The distribution of bonding environments comprised of the first nearest neighbors around a central atom was performed to study the prominence of different types of bonding structural units. As an example, a structural unit is represented as \underline{B} - B_5C_2 for the two-element system consists of a central atom B having its first nearest neighbors made up of five B atoms and two C atoms. From Figure 8 and 10 it is clear that the first nearest neighbor for B-atom for ReaxFF and New SW are around the same distance however C-atom have neighbors at different distances. These structural units are calculated using the cutoffs of 1.88 Å for B-B, 1.72 Å for B-C and 1.45 Å for C-C. The number of structural units fluctuates slightly based on the cutoffs used thus, values below 1% are ignored. Depending upon the type of crystal structure of boron carbide the presence of B-atom ranges from 80-87% and C-atom is 17-20%. The bonding environment of icosahedra can be analyzed mainly by boron centered structural units as shown in Figure 13.

In the crystal structure, structural unit \underline{B} - B_5 is mainly due to the pentagonal cap around the polar boron in icosahedral B_{12} . Similarly, \underline{B} - B_5C results from the icosahedral boron atom connecting with the carbon atom either via chain or any source and \underline{B} - B_6 arises from the fact that icosahedra are connecting each other through boron atoms. \underline{B} - B_4C and \underline{B} - B_4C_2 are the environments similar to \underline{B} - B_5 and \underline{B} - B_5C respectively except that the C-atom is within the icosahedra. Outside the icosahedra, boron centered environment can be found in the CBC chain in the form of structural unit \underline{B} - C_2 in the crystal boron carbide.

Figure 14 presents the local structural unit of Boron centered environment in the amorphous boron carbide samples prepared using New SW and ReaxFF potential. The boron centered environments without a carbon connection are slightly more likely in the New SW generated models evident from the <u>B</u>-B₃, <u>B</u>-B₄, <u>B</u>-B₅, <u>B</u>-B₆, <u>B</u>-B₇, and <u>B</u>-B₈ populations. The environment <u>B</u>-B₃ and <u>B</u>-B₄ are the results of distorted or even a few broken icosahedrons. The units <u>B</u>-B₅, <u>B</u>-B₆, <u>B</u>-B₇, and <u>B</u>-B₈ are the results of icosahedral presence and intra-icosahedral bonding through B-atoms. A structural unit containing carbon atoms seen in <u>B</u>-B₃C, <u>B</u>-

B₄C and B-B₅C are higher in ReaxFF generated structures. This indicates that the B-C bonding in the ReaxFF models is higher than the New SW which is reflected in their density in Table 5. This might be the result of B-C parameters in SW which requires further optimization than the parameter mixing rule.

5.2. Structure of amorphous boron carbide - HRMC

Short-range order present in the structure can be described by studying the nearest neighbor in the first coordination shell, bond length and the angular distribution function as bond angles [62]. The bond angle distribution $B(\theta)$ comparison between the MD and HRMC models is shown in Figure 15. The 3-membered characteristic ring present in the icosahedra is indicated by the bond angle peak at $\sim 60^{\circ}$ in all the models. The second kind of angle between two boron atoms in the icosahedra is B_R - B_G - B_G type forming between the second nearest neighbor of boron atoms. B_R - B_G - B_G gives rise to the second peak at $\sim 110^{\circ}$ which is seen in Figure 15. There is a small smooth peak around $\sim 160^{\circ}$ in the total $B(\theta)$ seen in all the amorphous models is due to some distorted and fragmented icosahedra. The total bond angle distribution of the HRMC models are very close in agreement with the MD generated amorphous models.

Figure 16 shows the radial distribution function of the amorphous models from HRMC and their comparison with the parent MD models. HRMC generated models are successful in fitting the g(r) peaks for almost all the peak positions. The peak fitting at the positions ~1.80Å, ~2.9Å and ~3.4Å shows icosahedrons are conserved in the HRMC models as in the MD generated models. Signal coming beyond the third nearest neighbor of B-B in the icosahedra is also reproduced and fitted accurately. The peak position at ~1.80Å is mainly attributed to B-B bonding which is less prominent in Figure 16 (c) compared to Figure 16 (a) although the number of boron atoms in both the cases is exactly the same. The reason behind this is the presence of C-atom in the icosahedra forming B₁₁C which keeps the number of B-atom constant but decreases the amount of B-B pair in the structure.

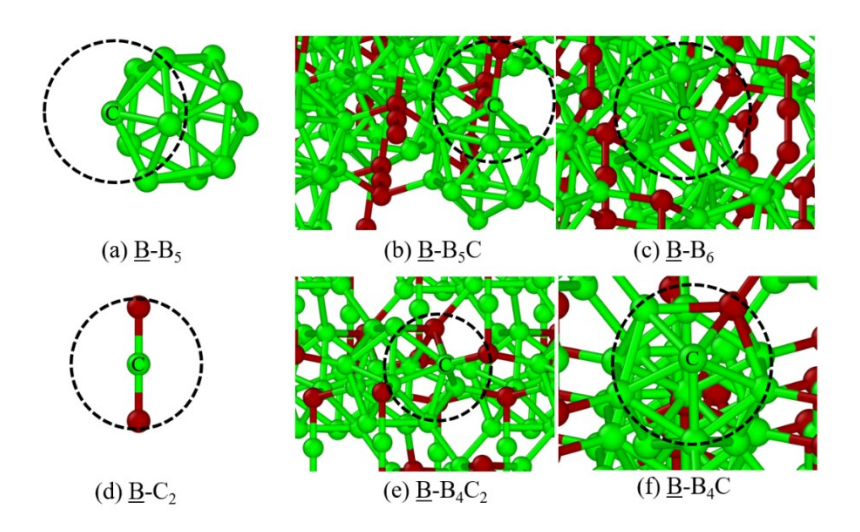


Figure 13 Some of the boron centered local structural environments present in the boron carbide crystal. Here green atoms are boron and brown atoms are carbon. The dotted circle is used to show the first neighbor environment around the boron center marked as C.

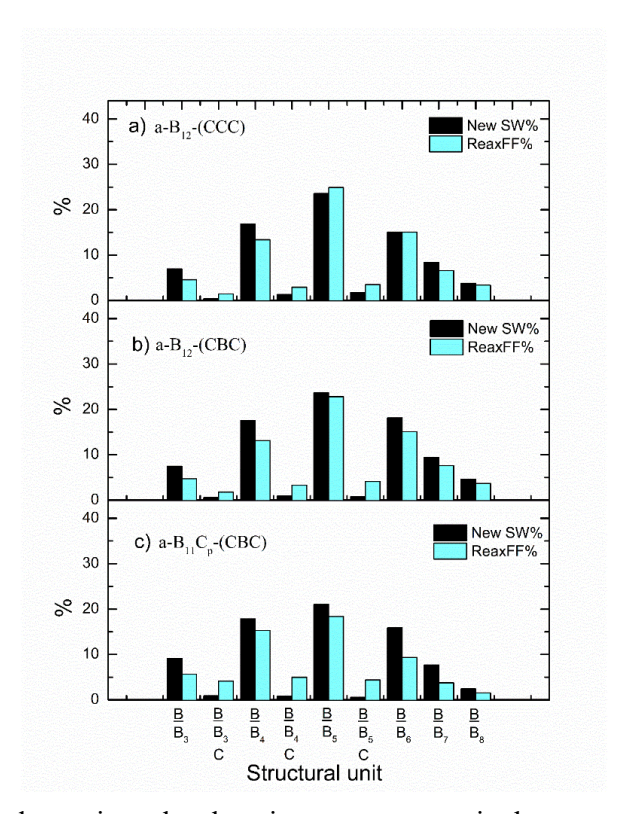


Figure 14 Boron centered prominent local environment present in the amorphous boron carbide models prepared using New SW and ReaxFF potential. (a) a-B₁₂-(CCC) (b) a-B₁₂-(CBC) and (c) a-B₁₁Cp-(CBC).

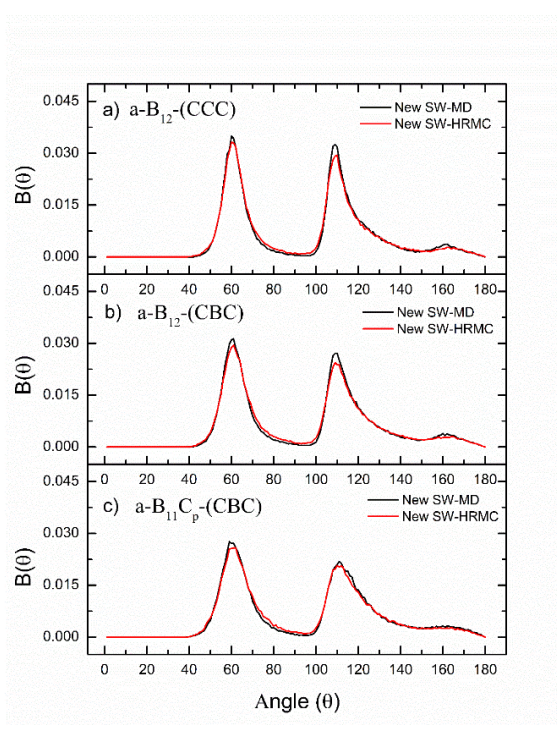


Figure 15 Bond angle distribution comparison between the amorphous models generated by MD and HRMC both using New SW potential. (a) $a-B_{12}$ -(CCC) (b) $a-B_{12}$ -(CBC) (c) $a-B_{11}C_p$ -(CBC).

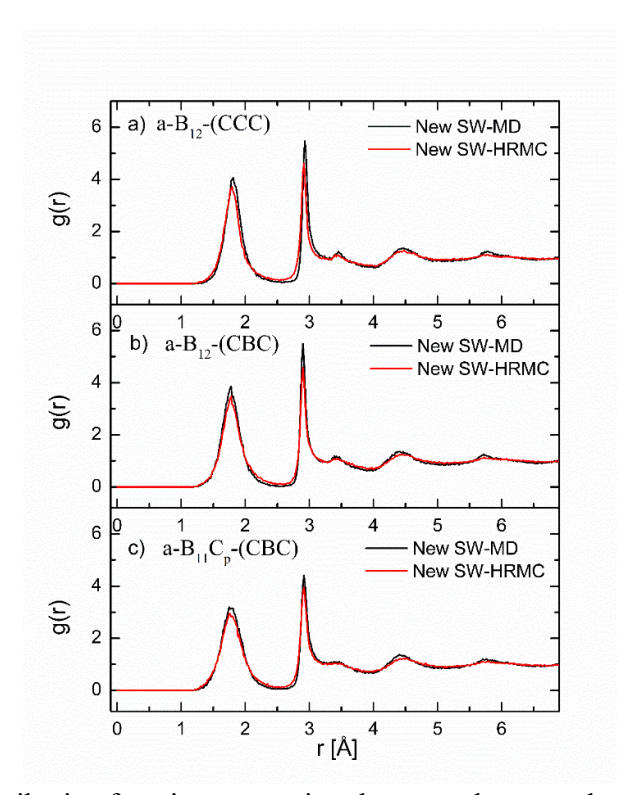


Figure 16 Radial distribution function comparison between the amorphous models generated by MD and HRMC both using New SW potential. (a) $a-B_{12}$ -(CCC) (b) $a-B_{12}$ -(CBC) (c) $a-B_{11}C_p$ -(CBC).

Static structure factor S(Q) fitting between the MD models and HRMC reconstructed structure is shown in Figure 17. Agreement with the MD diffraction data is very good except for the low Q region for the MD S(Q). The unphysical oscillations in the low Q region arise from Fast Fourier Transform (FFT) which can be controlled by no. of Q values to be fitted in the low Q region. The S(Q) signal intensity at \sim 4.9Å⁻¹ which is typical of Random B_{12} is underestimated in HRMC models in all the cases. However, all other secondary oscillating peaks are reproduced well.

The bonding environment is studied using the structural units around the first coordination shell of the central atom. Since boron atoms in our case are mostly present in the forms of the icosahedra boron centered environment, our amorphous models must take these into consideration and such clustering is of central importance. Figure 18 shows the structural unit of boron centered bonding environment comparison between the MD and HRMC generated structures. The structure is mainly dominated by <u>B</u>-B₃, <u>B</u>-B₄, <u>B</u>-B₅, and <u>B</u>-B₆ environment. The environments <u>B</u>-B₃ and <u>B</u>-B₄ are overestimated by HRMC however the higher coordinated environments like <u>B</u>-B₅, <u>B</u>-B₆, <u>B</u>-B₇, and <u>B</u>-B₈ are slightly underestimated. Carbon present first coordination environments <u>B</u>-B₃C, <u>B</u>-B₄C, and <u>B</u>-B₅C are less than 5% in the amorphous model which is seen in a similar proportion in the HRMC-generated structures. The coordination histogram is another constraint used to guide the HRMC simulation. Figure 19 shows the coordination distribution of boron atoms in the amorphous boron carbide structures. Boron atoms with four, five and six-fold coordination dominate the structure. HRMC simulation overestimates the three and four-fold coordination whereas higher coordinated boron atoms are underestimated. The five-fold coordination which is a signal of boron in the icosahedra is accurately seen in the HRMC structure compared to MD structures which ensure the stability of icosahedrons.

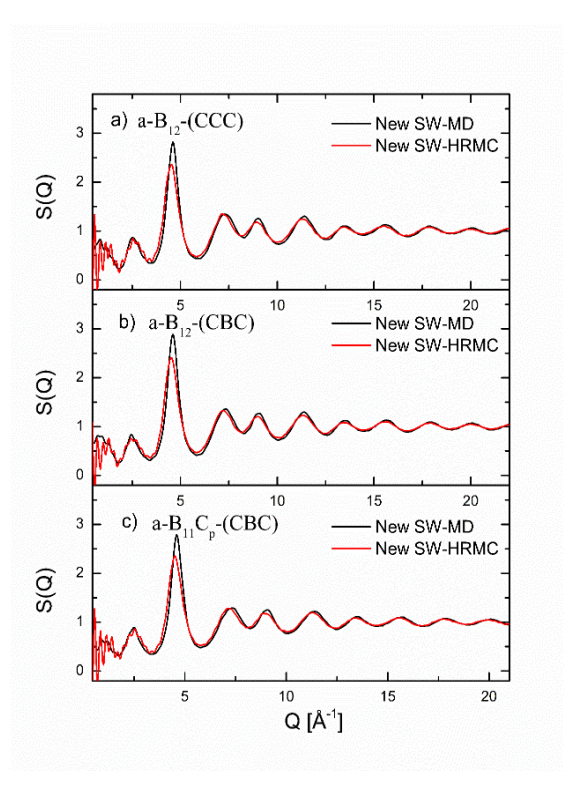


Figure 17 Static structure factor comparison between the amorphous models generated by MD and HRMC both using New SW potential. (a) a-B₁₂-(CCC) (b) a-B₁₂-(CBC) (c) a-B₁₁C_p-(CBC).

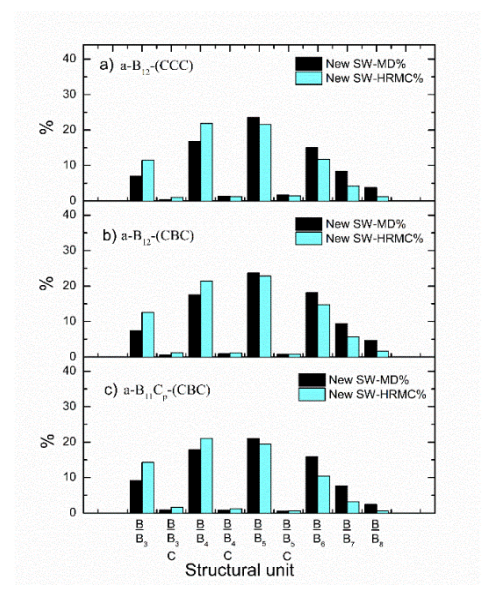


Figure 18 Boron centered prominent local environment present in the amorphous boron carbide models generated using MD and HRMC both using New SW potential (a) $a-B_{12}$ -(CCC) (b) $a-B_{12}$ -(CBC) and (c) $a-B_{11}$ Cp-(CBC.

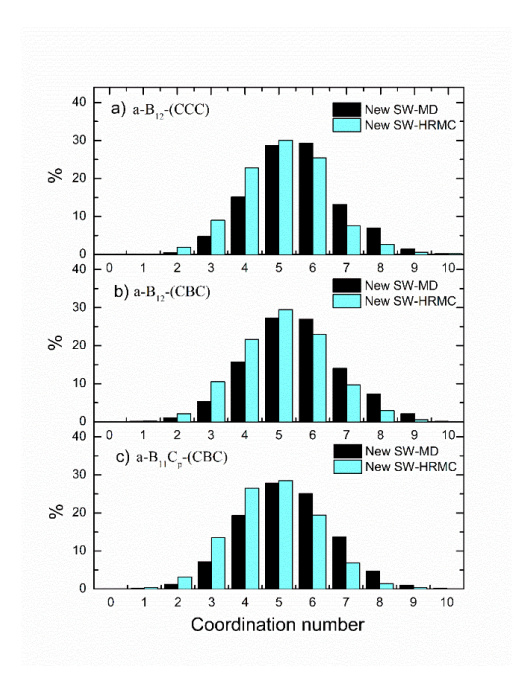


Figure 19 Coordination number distributions of Boron atoms in the amorphous models in MD and HRMC. (a) $a-B_{12}-(CCC)$ (b) $a-B_{12}-(CBC)$ (c) $a-B_{11}C_p-(CBC)$.

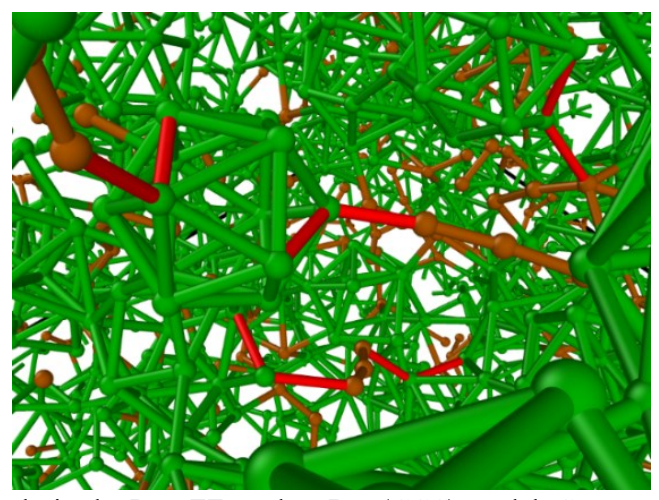


Figure 20 B-B-C angle in the ReaxFF made a- B_{12} -(CCC) model. Green atoms and bonds are the boron and brown atom and bonds are carbon. The red bond shows C atom bonding with B_{12} icosahedron's forming B-B-C angle.

Table 5 Density of the amorphous models using ReaxFF and New SW potential.

Amorphous Samples	B-atoms	C-atoms	Density-ReaxFF (gm/cm ³)	Density-New SW (gm/cm ³)
a-B ₁₂ -(CCC)	8748	2187	2.48	2.30
a-B ₁₂ -(CBC)	9477	1458	2.56	2.36
a-B ₁₁ Cp-(CBC)	8748	2187	2.53	2.37

6. Discussion

The density of all the final amorphous models of boron carbide from the Molecular Dynamics simulation is listed in Table 5. The literature value of density of α -rhombohedral boron is 2.476 gm/cm³ [40] which is close to the crystalline density 2.473 gm/cm³ [48] for B₁₂-(CCC). The ReaxFF generated a-B₁₂-(CCC) has a density of 2.48gm/cm³ which is similar to its crystalline counterpart and the amorphous model a-B_{2.5}C and the CVD prepared film by Pallier et. al [3]. Similarly, the density of a-B₁₁C_p-(CBC) using ReaxFF is found to be 2.53 gm/cm³ which is also very close to the reported crystalline density of 2.52 gm/cm³ [3,9]. However, the ReaxFF calculated density of a-B₁₂-(CBC) was the highest among all at 2.56 gm/cm³ which is also significantly higher than the crystalline density 2.44 gm/cm³ found in the literature [49]. The density of the amorphous models predicted by the New SW is 6-7% lower than that of ReaxFF models because of the slight increase in the interatomic distance between atoms e.g. C-C pair.

The bond angle distributions which are shown in Figures 6 and 7 produce relatively narrow and distinct peaks for New SW potential at ~ 110° whereas diffused peaks exist for the ReaxFF models which necessarily means more distorted icosahedrons are present in the amorphous sample prepared using ReaxFF. This prominent peak is due to the constraint in SW potential formulation where there is only one choice of the angular cutoff for three-body interaction which we choose to be a regular tetrahedral angle for B-B interaction. The same observation can be made in B-B-C angular type as well in Figures 6 and 7. ReaxFF sample has ~9.5 % of B-B-C angle which is ~4.7 % more than the New SW prepared sample. Since the B-B-C angle results from the bonding between the CCC carbon chain and the icosahedra, this could be

the reason behind the densified sample coming out of ReaxFF simulated amorphous models. Carbon atom bonding with icosahedral B_{12} is shown in Figure 20 for ReaxFF potential.

The B-B-C angle is much more prominent in the ReaxFF models of a-B12-(CBC) and a-B11Cp-(CBC) which can be attributed to more connectivity in the amorphous model helping in densifying the structure as seen from Table 5. The reason both a-B₁₂-(CBC) and a-B₁₁C_p-(CBC) are denser than a-B₁₂-(CCC) is that the C-atom in the edge of CBC chain can make three covalent bonds compared to only two in CCC chain. The increased affinity of C-atom in the CBC chain is responsible for an increased percentage of B-B-C angle due to their connectivity resulting in the denser structure. The consistently lower presence of B-B-C and C-B-B three-body angle in all the New SW generated model compared to the ReaxFF model could be the result of two body BC SW parameter. These two-body BC SW parameters were the results of parameter mixing rule and taken directly from Dugan et. al. [20] other than the σ parameter which affects the bond length and as seen from Table 3. The BC bond length due to New SW is very close to DFT and ReaxFF. Radial distribution function comparison of amorphous boron carbide for all the models shown in Figure 8 and Figure 10 shows the peaks at $\sim 1.8\text{Å}$, $\sim 2.9\text{Å}$, and shoulder at $\sim 3.4\text{Å}$ indicating the short-range order interaction strongly representing the icosahedrons. For pristine icosahedra's Larbi et. al. [52] mentioned the position of a second and third neighbor at 1.6*d and at 1.9*d respectively with "d" being the edge length in icosahedra. Pallier et. al. [3] found a similar result with peaks located at ~ 1.7 Å, ~ 2.9 Å, and ~ 3.4 Å. However, the first global peak is attributed to the B-C pair which is clearly dominated by B-B pair in our results. This arises from the fact that their model has longer chains of B and C atoms outside the icosahedrons whereas our models maintain the B/C stoichiometry with their crystalline counterpart with only short chained (CCC or CBC) atoms forming the matrix of B and C atoms. The RDF reported by Ivashchenko et. al. [14] in their first-principle study of a-120 generated from c-B₄C agrees with our amorphous models. But SRO study of a-B₄C by Bao et. al. [56] reported g(r) peaks at ~ 1.63 Å and ~ 2.95 Å without the shoulder peak at ~ 3.4 Å. Since the shoulder peak, ~ 3.4 Å is missing which is the indicator of unbroken icosahedra and their first peak shifted to ~ 1.63Å, more close to B-C bond length 1.57Å in the

amorphous matrix [3], our study suggests the thin films deposited had broken icosahedrons in the BC matrix. The a-B₄C thin film deposited at 600° C by Zhou et. al. reported a series of RDF peaks, namely ~ 1.4 Å originated from C-B-C chain, ~ 1.7 Å from the C-B intra-icosahedral bond length, ~ 2.9 Å from C-C in C-B-C, and a shoulder at ~ 3.5 Å. Our results from Figure 10 agree fairly well with the first two arguments although in our case the peak at 2.9Å is actually coming from the B-B instead of C-C pair. This is because the carbon concentration is only 20% which is relatively small to register into a major second nearest neighbor g(r) peak. Our study instead suggests that this peak should be attributed to the B-B second nearest neighbor in icosahedron which is also seen in other studies [3][56][52].

The results of the Wannier function Center (WFC) calculation of DFT generated a-B_{2.5}C [3] showing the B-B₆ and B-B₅C cluster environments which are also seen in our models in Figure 14. Simeone et. al [63] also attributed these environments in their NMR study of boron carbide. However B-B₄C₂ environment in our model isn't present in the appreciable amount as in a-B_{2.5}C. This could be due to the higher presence of C-atoms in their model (B/C= 2.5) compared to ours. Amorphous boron carbide mostly consists of fourfold coordinated boron's (B-B₃C, B-B₄), Penta-coordinated (B-B₄C, B-B₅) and hexacoordinated (B-B₅C, B-B₆) structural units with some presence of seven-fold (B-B₇) and eight-fold (B-B₈) coordinated boron centered units seen in Figure 14. The a-B_{2.5}C shows B-environment in the first coordination shell to be highest at six-fold coordination but our models have consistently shown a higher amount of five-fold coordination for both New SW and ReaxFF potentials. The difference in the chemical environment might be the result of different precursors used to get the amorphous networks as suggested by Ivashchenko [14].

7. Conclusion

We have performed MD simulations to study the short-range order present in the different variants of amorphous boron carbide using the SW and ReaxFF potentials. The existing SW potential of the boron cluster was optimized for α -rhombohedral boron and for B₁₂-(CCC), B₁₂-(CBC), and B₁₁C_p-(CBC) crystal structure based on their geometry. Amorphous models of boron carbide of three different variants were generated using New SW and ReaxFF and compared. The amorphous boron carbide models are fairly

peak generated by the New SW in g(r) and the bond angle at $\sim 110^{\circ}$ which is attributed to the limitation inherent in the interatomic SW formulation. The sophistication of ReaxFF allows a wide distribution of bonds and angles in the structure whereas the simplicity of SW limits the choices and sharpens the peaks. In our SRO study of a-B_xC, we were able to show that the presence of icosahedral structures can be recovered in part by utilizing the RDF peaks at ~ 3.4Å which is traced to the edge to edge Boron atom connections within the clusters. Similarly, a strong characteristic signal was also seen in the S(Q) near the vicinity of 4.5Å-1. The pentagonal cap in the icosahedra was discerned through the B-B₅ structural unit environment. In addition, we were able to differentiate between B₁₁C and B₁₂ icosahedrons in the amorphous structure via partial bond angle distribution of B-B-C. B₁₁C was found to have a sharp peak at ~60° which is nominal in B₁₂ present amorphous structures. SRO of a-B₁₂-(CCC), a-B₁₂-(CBC), and a- $B_{11}C_p$ -(CBC) were distinguishable based on BC pairs in g(r). a- B_{12} -(CCC) had no short bond peak at ~1.4Å coming to the chain atom and the intensity of split BC peaks was found to be higher in case of a-B₁₁C_p-(CBC) compared to a-B₁₂-(CBC) in ReaxFF models. However, the New SW potential couldn't differentiate between the BC pairs in chains and in icosahedral (inter- or intra-) bonding. Overall, the HRMC simulations utilizing the New SW potential were able to accurately reproduce the bonding environment, angular distribution, real and reciprocal space properties as in the parent MD models.

comparable in terms of peak positions and heights with the exception of a fairly sharp second neighbor

8. Acknowledgment

This research has been conducted by the support from National Science Foundation's (NSF) Designing Materials to Revolutionize and Engineer our Future (DMREF) program (Grant No. 1729176) and Department of Energy (DOE) National Energy Research Scientific Computing Center's (NERSC) computational support.

References

[1] H. Werheit, A. Leithe-Jasper, T. Tanaka, H.W. Rotter, K.A. Schwetz, Some properties of single-

- crystal boron carbide, J. Solid State Chem. 177 (2004) 575–579. doi:https://doi.org/10.1016/j.jssc.2003.04.005.
- [2] M. Beauvy, Stoichiometric limits of carbon-rich boron carbide phases, J. Less Common Met. 90 (1983) 169–175. doi:https://doi.org/10.1016/0022-5088(83)90067-X.
- [3] C. Pallier, J.-M. Leyssale, L.A. Truflandier, A.T. Bui, P. Weisbecker, C. Gervais, H.E. Fischer, F. Sirotti, F. Teyssandier, G. Chollon, Structure of an Amorphous Boron Carbide Film: An Experimental and Computational Approach, Chem. Mater. 25 (2013) 2618–2629. doi:10.1021/cm400847t.
- [4] F. Thévenot, Boron carbide—A comprehensive review, J. Eur. Ceram. Soc. 6 (1990) 205–225. doi:https://doi.org/10.1016/0955-2219(90)90048-K.
- [5] N. Hong, J. Mullins, K. Foreman, S. Adenwalla, Boron carbide based solid state neutron detectors: the effects of bias and time constant on detection efficiency, J. Phys. D. Appl. Phys. 43 (2010) 275101. doi:10.1088/0022-3727/43/27/275101.
- [6] N.S. Hosmane, J.A. Maguire, Z. Yinghuai, Polyhedral boron cage compounds: an account, Main Gr. Chem. 5 (2007) 251–265. doi:10.1080/10241220701607501.
- [7] M.M. Balakrishnarajan, P.D. Pancharatna, R. Hoffmann, Structure and bonding in boron carbide: The invincibility of imperfections, New J. Chem. 31 (2007) 473–485. doi:10.1039/B618493F.
- [8] Domnich Vladislav, Reynaud Sara, Haber Richard A., M. Chhowalla, Boron Carbide: Structure, Properties, and Stability under Stress, J. Am. Ceram. Soc. 94 (2011) 3605–3628. doi:10.1111/j.1551-2916.2011.04865.x.
- [9] H.K. Clark, J.L. Hoard, The Crystal Structure of Boron Carbide, J. Am. Chem. Soc. 65 (1943) 2115–
 2119. doi:10.1021/ja01251a026.
- [10] D.M. Bylander, L. Kleinman, S. Lee, Self-consistent calculations of the energy bands and bonding

- properties of B₁₂C₃, Phys. Rev. B. 42 (1990) 1394–1403. doi:10.1103/PhysRevB.42.1394.
- [11] S. Lee, D.M. Bylander, S.W. Kim, L. Kleinman, Computational search for the real tetragonal B₅₀, Phys. Rev. B. 45 (1992) 3248–3251. doi:10.1103/PhysRevB.45.3248.
- [12] D.R. Armstrong, J. Bolland, P.G. Perkins, G. Will, A. Kirfel, The nature of the chemical bonding in boron carbide. IV. Electronic band structure of boron carbide, B13C2, and three models of the structure B₁₂C₃, Acta Crystallogr. Sect. B. 39 (1983) 324–329. https://doi.org/10.1107/S0108768183002487.
- [13] S. Aydin, M. Simsek, Hypothetically superhard boron carbide structures with a B₁₁C icosahedron and three-atom chain, Phys. Status Solidi. 246 (2009) 62–70. doi:10.1002/pssb.200844328.
- [14] V.I. Ivashchenko, V.I. Shevchenko, P.E.A. Turchi, First-principles study of the atomic and electronic structures of crystalline and amorphous B₄C, Phys. Rev. B. 80 (2009) 235208.
- [15] R. Bao, D.B. Chrisey, Short range order structure of amorphous B₄C boron carbide thin films, J. Mater. Sci. 46 (2011) 3952–3959. doi:10.1007/s10853-011-5320-3.
- [16] I. Caretti, R. Gago, J.M. Albella, I. Jiménez, Boron carbides formed by coevaporation of B and C atoms: Vapor reactivity, B _xC_{1-x} composition, and bonding structure, Phys. Rev. B. 77 (2008) 174109.
- [17] K. Shirai, S. Emura, S. Gonda, Y. Kumashiro, Infrared study of amorphous B_{1-x}C_x films, J. Appl. Phys. 78 (1995) 3392.
- [18] X.Q. Yan, W.J. Li, T. Goto, M.W. Chen, Raman spectroscopy of pressure-induced amorphous boron carbide, Appl. Phys. Lett. 88 (2006) 131905. doi:10.1063/1.2189826.
- [19] D. Ghosh, G. Subhash, C.H. Lee, Y.K. Yap, Strain-induced formation of carbon and boron clusters in boron carbide during dynamic indentation, Appl. Phys. Lett. 91 (2007) 61910. doi:10.1063/1.2768316.

- [20] N. Dugan, Ş. Erkoç, Structural properties of boron carbide nanoparticles: Application of a new set of Stillinger–Weber parameters, Comput. Mater. Sci. 50 (2011) 2950–2954. doi:10.1016/J.COMMATSCI.2011.05.012.
- [21] F.H. Stillinger, T.A. Weber, Computer simulation of local order in condensed phases of silicon, Phys. Rev. B. 31 (1985) 5262–5271. doi:10.1103/PhysRevB.31.5262.
- [22] F.F. Abraham, I.P. Batra, Theoretical interpretation of atomic-force-microscope images of graphite, Surf. Sci. 209 (1989) L125–L132. doi:10.1016/0039-6028(89)90053-8.
- [23] P. Mahon, B.A. Pailthorpe, G.B. Bacskay, A quantum mechanical calculation of interatomic interactions in diamond, Philos. Mag. B. 63 (1991) 1419–1430. doi:10.1080/13642819108205571.
- [24] P.B. Rasband, P. Clancy, B.W. Roberts, Tight-binding studies of the tendency for boron to cluster in c-Si. I. Development of an improved boron–boron model, J. Appl. Phys. 84 (1998) 2471–2475. doi:10.1063/1.368408.
- [25] W.H. Moon, H.J. Hwang, A modified Stillinger–Weber empirical potential for boron nitride, Appl. Surf. Sci. 239 (2005) 376–380. doi:10.1016/J.APSUSC.2004.05.284.
- [26] X. Deng, Y. Song, J. Li, Y. Pu, Parametrization of the Stillinger-Weber potential for Si/N/H system and its application to simulations of silicon nitride film deposition with SiH₄/NH₃, J. Appl. Phys. 115 (2014) 54902. doi:10.1063/1.4863841.
- [27] X.W. Zhou, R.E. Jones, K. Chu, Polymorphic improvement of Stillinger-Weber potential for InGaN,
 J. Appl. Phys. 122 (2017) 235703. doi:10.1063/1.5001339.
- [28] X.W. Zhou, D.K. Ward, J.E. Martin, F.B. van Swol, J.L. Cruz-Campa, D. Zubia, Stillinger-Weber potential for the II-VI elements Zn-Cd-Hg-S-Se-Te, Phys. Rev. B. 88 (2013) 85309. doi:10.1103/PhysRevB.88.085309.
- [29] S. Plimpton, Fast Parallel Algorithms for Short-Range Molecular Dynamics, J. Comput. Phys. 117

- (1995) 1–19. doi:https://doi.org/10.1006/jcph.1995.1039.
- [30] L. Pizzagalli, J. Godet, J. Guénolé, S. Brochard, E. Holmstrom, K. Nordlund, T. Albaret, A new parametrization of the Stillinger-Weber potential for an improved description of defects and plasticity of silicon, J. Phys. Condens. Matter. 25 (2013) 55801. doi:10.1088/0953-8984/25/5/055801.
- [31] G. Opletal, T.C. Petersen, B. O'Malley, I.K. Snook, D.G. McCulloch, I. Yarovsky, HRMC_1.1: Hybrid Reverse Monte Carlo method with silicon and carbon potentials, Comput. Phys. Commun. 182 (2011) 542. doi:10.1016/J.CPC.2010.10.023.
- [32] T. Petersen, B. O'Malley, I. Snook, D.G. McCulloch, N.A. Marks, I. Yarovsky, Hybrid approach for generating realistic amorphous carbon structure using metropolis and reverse Monte Carlo AU Opletal, George, Mol. Simul. 28 (2002) 927–938. doi:10.1080/089270204000002584.
- [33] T. Petersen, I. Yarovsky, I. Snook, D.G. McCulloch, G. Opletal, Structural analysis of carbonaceous solids using an adapted reverse Monte Carlo algorithm, Carbon N. Y. 41 (2003) 2403–2411. doi:10.1016/S0008-6223(03)00296-3.
- [34] G. Opletal, T.C. Petersen, D.G. McCulloch, I.K. Snook, I. Yarovsky, The structure of disordered carbon solids studied using a hybrid reverse Monte Carlo algorithm, J. Phys. Condens. Matter. 17 (2005) 2605–2616. doi:10.1088/0953-8984/17/17/008.
- [35] G. Opletal, T.C. Petersen, I.K. Snook, D.G. McCulloch, Modeling of structure and porosity in amorphous silicon systems using Monte Carlo methods, J. Chem. Phys. 126 (2007) 214705. doi:10.1063/1.2743029.
- [36] G. Opletal, T.C. Petersen, I.K. Snook, S.P. Russo, HRMC_2.0: Hybrid Reverse Monte Carlo method with silicon, carbon and germanium potentials, Comput. Phys. Commun. 184 (2013) 1946–1957. doi:10.1016/j.cpc.2013.03.004.

- [37] G. Opletal, T.C. Petersen, B. O'Malley, I.K. Snook, D.G. McCulloch, I. Yarovsky, HRMC: Hybrid Reverse Monte Carlo method with silicon and carbon potentials, Comput. Phys. Commun. 178 (2008) 777–787. doi:10.1016/J.CPC.2007.12.007.
- [38] P.B. Rasband, P. Clancy, M.O. Thompson, Equilibrium concentrations of defects in pure and B-doped silicon, J. Appl. Phys. 79 (1996) 8998–9011. doi:10.1063/1.362632.
- [39] Y. Şimsek, Ş. Erkoç, Structural Properties of Monolayer Boron Carbide Nanoribbons Under Strain:

 Molecular Dynamics Simulations, J. Comput. Theor. Nanosci. 12 (n.d.) 2180–2188.

 https://www.ingentaconnect.com/content/asp/jctn/2015/00000012/00000009/art00025.
- [40] K. Persson, Materials Data on B (SG:166) by Materials Project, (2014). doi:10.17188/1191505.
- [41] B.F. Decker, J.S. Kasper, The crystal structure of a simple rhombohedral form of boron, Acta Crystallogr. 12 (1959) 503–506. https://doi.org/10.1107/S0365110X59001529.
- [42] K. Katada, An Electron Diffraction Study Evaporated Boron Films, Jpn. J. Appl. Phys. 5 (1966) 582–587. doi:10.1143/jjap.5.582.
- [43] X. Wu, J. Dai, Y. Zhao, Z. Zhuo, J. Yang, X.C. Zeng, Two-Dimensional Boron Monolayer Sheets, ACS Nano. 6 (2012) 7443–7453. doi:10.1021/nn302696v.
- [44] D.L.V.K. Prasad, E.D. Jemmis, Stuffing Improves the Stability of Fullerenelike Boron Clusters, Phys. Rev. Lett. 100 (2008) 165504. doi:10.1103/PhysRevLett.100.165504.
- [45] T.B. Tai, M.T. Nguyen, A new chiral boron cluster B₄₄ containing nonagonal holes, Chem. Commun. 52 (2016) 1653–1656. doi:10.1039/C5CC09111J.
- [46] D. Berthelot, Sur le mélange des gaz, Comptes Rendus Hebd. Des Séances. 126 (1898) 1703–1855.
- [47] LAMMPS Pair Styles, (2019). https://lammps.sandia.gov/doc/pair_sw.html (accessed January 5, 2019).

- [48] K. Persson, Materials Data on B₄C (SG:166) by Materials Project, (2016). doi:10.17188/1285041.
- [49] K. Persson, Materials Data on B₁₃C₂ (SG:166) by Materials Project, (2014). doi:10.17188/1276602.
- [50] Q. An, W.A. Goddard, Atomistic Origin of Brittle Failure of Boron Carbide from Large-Scale Reactive Dynamics Simulations: Suggestions toward Improved Ductility, Phys. Rev. Lett. 115 (2015) 105501. doi:10.1103/PhysRevLett.115.105501.
- [51] L. Martínez, R. Andrade, E.G. Birgin, J.M. Martínez, PACKMOL: A package for building initial configurations for molecular dynamics simulations, J. Comput. Chem. 30 (2009) 2157–2164. doi:10.1002/jcc.21224.
- [52] M. Belhadj-Larbi, R.C. Horn, P. Rulis, Model creation and electronic structure calculation of amorphous hydrogenated boron carbide: a classical/ab initio hybrid approach, RSC Adv. 7 (2017) 46788–46795. doi:10.1039/C7RA06988J.
- [53] A.H. Farmahini, G. Opletal, S.K. Bhatia, Structural Modelling of Silicon Carbide-Derived Nanoporous Carbon by Hybrid Reverse Monte Carlo Simulation, J. Phys. Chem. C. 117 (2013) 14081–14094. doi:10.1021/jp403929r.
- [54] T.X. Nguyen, S.K. Bhatia, S.K. Jain, K.E. Gubbins, Hybrid Reverse Monte Carlo Reconstruction and Simulation Studies, in: 2006 Int. Conf. Nanosci. Nanotechnol., 2006: p. 1. doi:10.1109/ICONN.2006.340708.
- [55] G. Opletal, T.C. Petersen, A.S. Barnard, S.P. Russo, On reverse Monte Carlo constraints and model reproduction, J. Comput. Chem. 38 (2017) 1547–1551. doi:10.1002/jcc.24799.
- [56] R. Bao, D.B. Chrisey, Short range order structure of amorphous B₄C boron carbide thin films, J. Mater. Sci. 46 (2011) 3952–3959. doi:10.1007/s10853-011-5320-3.
- [57] A. Bouzid, S. Le Roux, G. Ori, M. Boero, C. Massobrio, Origin of structural analogies and differences between the atomic structures of GeSe₄ and GeS₄ glasses: A first principles study, J.

- Chem. Phys. 143 (2015) 34504. doi:10.1063/1.4926830.
- [58] M. Celino, S. Le Roux, G. Ori, B. Coasne, A. Bouzid, M. Boero, C. Massobrio, First-principles molecular dynamics study of glassy GeS₂:Atomic structure and bonding properties, Phys. Rev. B. 88 (2013) 174201. doi:10.1103/PhysRevB.88.174201.
- [59] Z. Chaker, G. Ori, C. Tugène, S. Le Roux, M. Boero, C. Massobrio, E. Martin, A. Bouzid, The role of dispersion forces on the atomic structure of glassy chalcogenides: The case of GeSe₄ and GeS₄, J. Non. Cryst. Solids. 499 (2018) 167–172. doi:https://doi.org/10.1016/j.jnoncrysol.2018.07.012.
- [60] Y. Sakaguchi, T. Hanashima, K. Ohara, A.-A.A. Simon, M. Mitkova, Structural transformation in Ge_xS_{100-x} (10<x<40) network glasses: Structural varieties in short-range, medium-range, and nanoscopic scale, Phys. Rev. Mater. 3 (2019) 35601. doi:10.1103/PhysRevMaterials.3.035601.
- [61] N. Fueki, T. Usuki, S. Tamaki, H. Okazaki, Y. Waseda, Structure of Amorphous Ge–S System by X-Ray Diffraction, J. Phys. Soc. Japan. 61 (1992) 2814–2820. doi:10.1143/JPSJ.61.2814.
- [62] A.A. Babaev, Short- and medium-range order in disordered systems, Bull. Russ. Acad. Sci. Phys. 74 (2010) 677–679. doi:10.3103/S1062873810050266.
- [63] D. Simeone, C. Mallet, P. Dubuisson, G. Baldinozzi, C. Gervais, J. Maquet, No Title, J. Nucl. Mater. 277 (2000) 1.